Passivity and pitting corrosion of carbon steel in chloride containing borate buffer solution

A thesis submitted in partial fulfilment of the requirements for the degree of

M. Tech Dual degree

by

Yogesh Kumar Modi
(Roll No. – 710MM1095)

Department of Metallurgical and Materials Engineering
National Institute of Technology
Rourkela – 769008, Odisha
India

May 2015

Department of Metallurgical and Materials Engineering, National Institute of Technology, Rourkela – 769008, Odisha, India

CERTIFICATE

This is to certify that the thesis entitled "**Passivity and pitting corrosion studies of carbon steel in chloride containing borate buffer solution"** submitted by **Yogesh Kumar Modi** to National Institute of Technology, Rourkela is a record of bonafide research work under our supervision and is worthy of consideration for the award of the degree of Integrated B. Tech and M. Tech of the Institute. The candidate has fulfilled all prescribed requirements for the thesis, which is based on candidate's own work, has not been submitted elsewhere for a degree or diploma.

Prof. Archana Mallik
Supervisor
Assistant Professor

Acknowledgment

This project was carried out at National Institute of Technology, Rourkela under a span of 2 years, which undertook a lot of effort and help from different persons, without whom this research work wouldn't have been as fruitful as it is, and I would like to extend my deepest gratitude to all of them for making me what I am today.

First of all, my supervisor, Prof. Archana Mallik, as dynamic as is her personality, she is one of the kind hearted person I have ever met. Her need to keep me innovative and punctual had brought in me vivid changes which I will explore throughout my life, She is what we say the teacher of "Modern times", unravelling in me the science. Madam, I have been a little insincere and casual yet you have been patient, you made me realise the importance of little things, significance of literature and design in technology and of all to be patient. From the core of my heart, I would like to thank you, for your constant support and encouragement and I really look forward to work with you in the near future.

I am grateful to my co-supervisor Prof. Anandiya Basu for his supervision and support in carrying out this project.

I am also thankful to Prof. U. K. Mohanty, for he has been there as a family to me, supporting and encouraging my causes.

I would like to thank the laboratory members of Department of Metallurgical and Materials Engineering, NIT Rourkela.

Now to the members of our lab, RamKumar, Sumant, Prekshya and Rajneesh, guys talking to you all was a piece of cake, you were always there, alleviating the pressure of the rigorous work. Thank you all!! It was a time well spent.

I would like to express my deepest gratitude to my parents, Pramod Kumar Modi and Sangita Modi, who have always been supporting me in my studies. Thanks for your love and support!

I am grateful to Amrita Gokhale, the light in darkness, for her constant support and your sometime annoying need to correct my English. And to my wonderful friends, Punit, Ravindra, Aishwarya, Alok and Chinu. Thank you guys for keeping me cheerful and happy.

All errors and limitations remaining in this thesis are mine alone.

Yogesh Kumar Modi
(May 2015)

Abstract

Passivation is the formation of oxide layer on metals which protects the underlying metal from corrosion. The breakdown of this protective layer due to various environmental effects leads to rapid corrosion, restricting the metal use in long term purposes, and hence a study of passivity breakdown allows for the optimisation of process parameter and environmental constraints for extending the lifetime of usefulness of the metal.

Passivity breakdown of high manganese steel in deaerated borate buffer solution has been studied in the following thesis. The steel used here is a special high strength C-Mn steel used extensively in pressure vessels. This article describes an attempt to predict and interpret the pitting corrosion of the steel in terms of the point defect model (PDM) in deaerated borate buffer solution at different pH (6, 8, 9, 10) at different chloride ion concentration ($[Cl^-]$ = 0.01, 0.1, 0.6, 1M). The objectives of the work is to study the state of passivity and the related characteristics, determine the breakdown potential (V_c) as functions of pH, chloride concentration and potential sweep rate (υ), analyze the relationship between V_c and $[Cl^-]$, pH and scan rate (v) in terms of PDM to extract parameter values for passivity breakdown and assess the ability of PDM to account for passivity breakdown.

The passive film was found to contain n-type defect with film thickness depending directly on the passivation potential. The near normal distribution in breakdown potential is in satisfactory agreement with the analytical prediction of the breakdown potential distribution obtained from PDM. The linear dependence of breakdown potential on the square root of potential scan rate and polarizability dependence of the barrier layer/solution interface upon potential and pH are 0.83 and - 0.01 respectively, as predicted by the PDM, yields an estimate of the critical areal concentration of condensed vacancies at the metal/film interface (ξ =

4.9×10^{14} cm^{-2}) that leads to passivity breakdown. The value of the critical areal concentration of condensed vacancies falls in well agreement with the value obtained from structural argument. These provide convincing evidence for the validity of PDM for modelling passivity breakdown on high manganese carbon steel

Keywords:

High manganese carbon steel, Breakdown potential, Borate buffer, Point defect model, Potentiodynamic curves, Critical areal concentration of vacancies, Normal distributions,

Contents Page No.

Nomenclature

F	Faraday constant
R	Universal gas constant
T	Absolute Temperature
Nv	Avogadro's number
χ	The film layer stoichiometry
Ω	Molar volume of Fe_2O_3 per cation
D	The mean cation vacancy diffusivity
σD,	The standard deviation for D
α,	Potential dependence of $\varphi f/s$
ε,	The electric field strength
ξ,	The critical vacancy concentration
Jm,	The critical vacancy flux
β	pH dependence of $\varphi_{f/s}$
v	Scan rate
Vc	Breakdown potential
a_{cl-}	Chloride concentration
j	Current density
Jca	Cationic flux
Ja	Anionic flux
n	Electrons
h	holes
$V_M^{x\prime}$	Cation vacancy
$V_o^{\blacksquare\blacksquare}$	Anion vacancy
M	Metal atom
v_m	Metal holes

Abbreviations

PDM	Point defect model
SCE	Saturated Calomel Electrode
WE	working electrode
CE	Counter electrode

List of figures

List of Tables

Chapter 1

Introduction

1.1. Background

Unprecedented technological transformation were swept in to our civilisations with the discovery of metals of which Iron is one of the most significant metal in terms of use and availability. With the passage of time, humans learn to smelt and cast iron which led to Industrial revolution. The mastering of iron and steel manufacturing resulted in designing of complex machines and infrastructure which are still evolving at light speed. Other metals like

Aluminium, magnesium, zirconium, and titanium having high specific strength were obtained from their ores by using electrochemical techniques. The development of these metals resulted in diverse applications ranging from nuclear applications to a razor blade, aircraft industry to automobile manufacturing. The discovery and development of metals is one of the cornerstone, just like the discovery of fire and wheel was in the history of human life, and it makes the world habitable and safe as it is today.

Iron, used extensively in almost all the modern equipment, forms the backbone of today's modern industrial world, is found in nature in oxidised form and hence, reduction is carried out to get pure iron. The other reactive metal like Aluminium, magnesium and titanium also plays an equally important role. These metals very readily react with oxygen and water when exposed to environment leading to the phenomena of corrosion, which results in disintegration of metal property and stability. Yet these metals are considered among the most useful metal when they can so readily react with the environment to undergo corrosion. The answer to this question lies in the amazing, remarkable and extraordinary, yet still unclear theory of "passivity" [1].

Passivity is the formation of stable, thin, adherent oxide layer (mainly) which imparts immediate kinetic stability to reactive metal. It was first discovered by Faraday while conducting experiments of Iron in nitric acid, which showed iron corroding in dilute medium while no corrosion took place in concentrated nitric acid. This anomaly gave way to the theory and discovery of passivation in highly oxidising solution as is concentrated nitric acid [2-3]. This observation was understood with the development of the electrochemical thermodynamic diagrams by Pourbaix [4]. This oxide layer protects the underlying metal from the nearby surrounding and inhibits corrosion, but this passivated layer is subjected to breakdown

uniformly or locally depending on the environmental constraints [5]. Once broken, the metal will face extensive dissolution leading to failure of the metal use.

The stability and kinetics of the formation of the passivated layer has been studied since its inceptions and they are still various aspects of it that remains unaccounted. Various model were developed since 1930 by various scientists to account for the above but still not all the aspects were justified, until 1990 when Point Defect Model was developed. The point defect model successfully accounted for the passivity and passivity breakdown of the films in various solution on various metals. This model was developed with time, which resulted in the formation of three generations which gradually removed all the errors of the previous generation.

1.2. **Research motivation**

The high manganese carbon steel is extensively used in pressure vessels in nuclear power plants for storage of used nuclear fuel in large containers buried deep in the ground. This steel containers are in constant contact with underground running water under high pressure. With time these conditions renders the metals susceptible to corrosion and disintegration of the structure. According to the Government rules for nuclear industries, the life of these metals should be in the range of 100000 to 1000000 years for successful implementation. Hence, thus study simulates the environmental condition of nuclear industry in laboratory conditions and testing the stability of the oxide films under the extreme conditions.

The results obtained from the different experiments conducted are then extrapolated to study the stability of these metals containers for the 100000 to 1000000 years as per the government

requirement. Thus, this study will give a clear idea about the behaviour of the metals containers under these extreme conditions and an idea about the safety limits to be installed in the nuclear plants to avoid the immense risk of radiation associated with the nuclear power plants. This will also make possible carefree storage of the waste nuclear fuels and reusing them for better sustenance and saving natural resources by recycling.

1.3. Objectives

The objective of this study is an attempt to predict and interpret the pitting corrosion of the steel in terms of the point defect model (PDM) in deaerated borate buffer solution at different pH (6, 8, 9, 10) at different chloride ion concentration ($[Cl^-]$ = 0.01, 0.1, 0.6, 1M).

The outline of the work is to:

(i) To study the state of passivity and the related characteristics :

Passive region, Passive layer thickness and current, Defect type and concentration

(ii) To determine the breakdown potential (V_c) as functions of pH, chloride concentration and potential sweep rate (υ);

(iii) To analyse the relationship between V_c and $[Cl^-]$, pH and υ in terms of PDM to extract parameter values for passivity breakdown and

(iv) To plot the near normal distribution in breakdown potential obtained experimentally with the analytical prediction of the breakdown potential distribution obtained from PDM.

(v) To assess the ability of PDM to account for passivity breakdown.

The objectives were achieved by plotting various potentiodynamic curves at different pH and chloride concentrations and using the slope of these curves to evaluate the various process parameters as described the Point defect model. Once the parameters were obtained, a computational modelling was done to plot cumulative probability distribution plot using PDM

which was compared with the experimentally obtained data. The amount of analogy obtained then gave the idea about the accountability of the PDM to assess the passivity breakdown on high manganese carbon steel in deaerated chloride containing borate buffer solution.

1.4. Structure of the thesis

This thesis has been divided into 5 chapters. In Chapter 2, the importance of passivity and the basics of passivity breakdown is explained followed by the development and the basic outline of the Point defect model and the approach with which Point defect model explains passivity breakdown on steel in chloride containing solutions. Insights about pitting corrosion are also sighted

Chapter 3 deals with the experimental aspects, which includes polishing of the samples, preparation of the chloride containing borate buffer, electrochemical setup, plotting of various potentiodynamic curves with varying chloride concentration, pH and potential sweep rate, optical microscopy. The computational modelling is done using the data obtained from the above experiments

Chapter 4 summarises the conclusion obtained during the experimentation like the V-I plot with varying chloride concentration and pH. The slope of this curve gave the various parameter that was used for modelling the passivity breakdown. The cumulative probability distribution of the breakdown potential obtained from experimental data was plotted and compared with the plot obtained from PDM. There was sufficient evidence of the validity of PDM in explaining the passivity and passivity breakdown on 760 SOHIC carbon steel in deaerated chloride containing borate buffer solution.

An abridgement of this dissertation is sighted in Chapter 5

Chapter 2

Literature survey

This chapter gives a brief insight on corrosion and specifically localised pitting corrosion. Section 2.1 is a summary of the various type of corrosion, passivation and mechanism of pitting corrosion in the presence of aggressive chloride ions. Section 2.2 cites the development of computational modelling in the field of passivation and the various models made to address the passivity. Section 2.3 highlights the basic assumptions of point defect model followed by mathematical formulation and modelling

2.1 Significance of corrosion

Corrosion is the destruction of the metal upper surface due to chemical reactions between a metal/alloy and its environment. Every metal is found in nature in its combined from known

as minerals and a certain amount of energy is invested for their extraction from their minerals. This same amount of energy is liberated during the use of metal in its extracted form by chemical reactions with the surrounding environment. This renders the phenomena of corrosion. Therefore, corrosion is the existence of the tendency of the metal to return to its parent form, from which it was extracted. Hence, corrosion is extractive metallurgy in reverse [6].

Corrosion can manifest itself in different ways with each having certain specific characteristics and property. Almost everybody once in their life time have a personal experience with the phenomena of corrosion. I myself was intrigued to find the nuts of my specs getting corroded in rainy season. The rusting of iron is the most common phenomena of corrosion in our daily life. Leaking of the water heater, holes in the body parts of various equipment, abnormal breakage of sewer lines are some of the examples of different types of corrosion in your daily life. This is not the end, the scope of corrosion lies to great extent, and the disasters due to corrosion results in large scale loss of human lives accompanied with economic losses.

We are very much familiar with the measures taken to combat different forms of corrosion. Automobile industries spent millions of dollars every year on after-market corrosion protection for the prevention of the dreaded rust appearance on the exteriors of the automobile. Extensive research and development is done in the development inherent corrosion resistant property in metals. Development of stainless steel, corrosion resistance grade steel, has great importance in today's world. It uses ranges from household utensils to large scale container used for storing spent nuclear fuels. Coating of steels known as galvanization greatly delays the corrosion of steels. The economic cost of combating various form of corrosion ranges between $8 billion and $126 per year in United States of America alone [7].

The turbine blades used in electric power plants requires costly alloy to minimise degradation. Nuclear power plants demands extensive and elaborate treatment systems for cooling water and steam to minimise the risk of corrosion. The petroleum industry is plagued with corrosion problems which can be disastrous if proper care and attention is not given to inhibit the corrosion. The power generation facility are also too prone to immediate deterioration due to involvement of high temperature during the process of production. The deterioration of the bridges and public structures are accelerated by the corrosion of the steel in the concrete.

2.2 Mechanism of aqueous corrosion

All metallic corrosion involves charge transfer in aqueous solution and hence it is necessary to understand he electrochemical nature of corrosion. Let us consider an example of corrosion between zinc and hydrochloric acid given by the reaction.

$Zn + 2HCl \rightarrow ZnCl_2 + H_2$

Zinc reacts with hydrochloric acid to from zinc chloride and release hydrogen gas on the surface. The above reaction can be separated in two parts as follows:

$Zn \rightarrow Zn^{2+} + 2e^-$ Anodic reaction

$2H^+ + 2e^- \rightarrow H_2$ Cathodic reaction

Anodic reaction is the oxidation reaction whereby zinc valence increases from 0 to +2 liberating electrons, and the cathodic reaction is a reduction reaction whereby hydrogen ions gets reduced to hydrogen gas accepting electrons.

The composite reaction involving electronic charge transfer is shown in Figure 2.1.

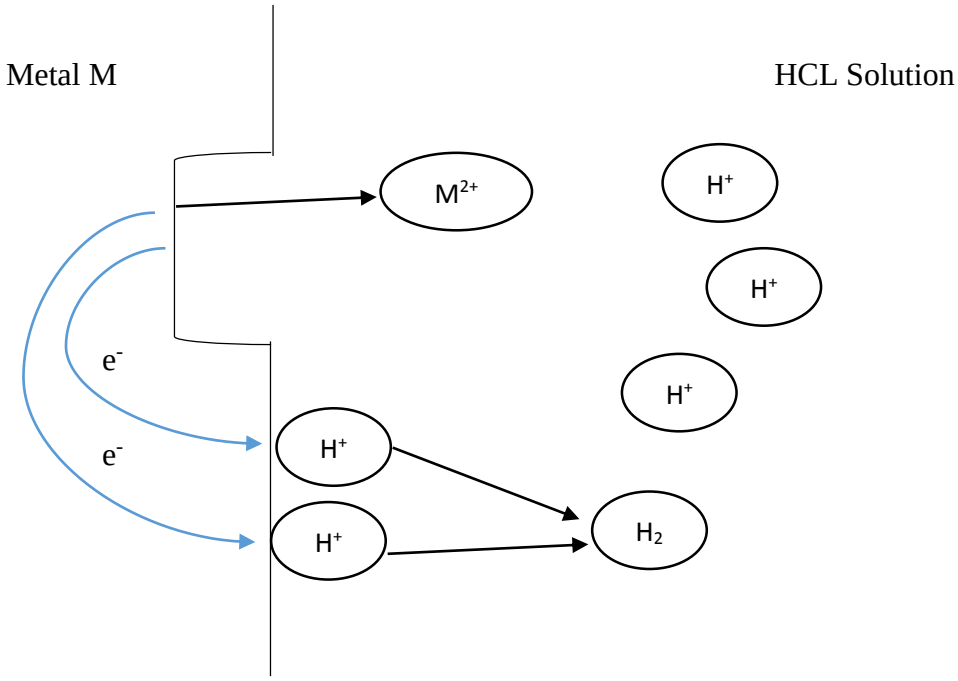

Fig 2.1 Schematic diagram of metal M dissolution giving metal ion and metal electrons, which are consumed by during reduction of hydrogen ion to hydrogen gas.

The transfer of electronic charge requires a medium which is called electrolyte. In most of the natural cases such as rusting of iron water acts as an electrolyte. Hence, all aqueous corrosion requires transfer of electronic charge. Transfer of electrons is equally important for the above reactions to take place. If by some method extra electrons are supplied to the metal in Fig 2.1, the rate of metal dissolution and anodic reaction will decrease but the liberation if hydrogen gas and cathodic reaction will increase. Hence application of negative potential with the supply of electron decreases the rate of corrosion. This is the basis of cathodic protection used extensively for the protection of underground pipelines, steel tanks etc. Fewer number of cathodic reductions reactions are seen in practical application of which hydrogen reduction occurs almost inevitably in all acid solutions.

2.2.1 Polarization

All electrochemical reactions, as the one taking place during corrosion, occurs at certain finite rate. These rate of reactions can be altered by the use of external application. As mentioned above if extra electrons are made available at the surface of the metal, then there is a existence of negative charge due to accumulation of electrons which are waiting for reactions at the surface. Hence, the rate of the reaction is limited as all the electrons are not accommodated for the reactions. This negative potential alteration is known as cathodic polarization. Similarly a positive potential made by removing electrons on the metal surface so as to make it electron deficient can also be achieved which is termed as anodic polarization. During equilibrium the rate of cathodic and anodic reactions are equal and hence to compensate, more and more dissolution of metal will occur to supply for the equivalent amount of electrons to account for the cathodic reactions and hence tendency for dissolution increases. Anodic polarization thus represent a driving force corrosion. A steady state potential as mentioned above, denoted by Ecorr, is achieved in aqueous solution which is determined by the ability of the anodic and cathodic reactions to exchange electrons. Any potential applied higher than Ecorr will result in accelerated corrosion rate as shown in figure 2.2. €= E- Ecorr is the anodic polarisation.

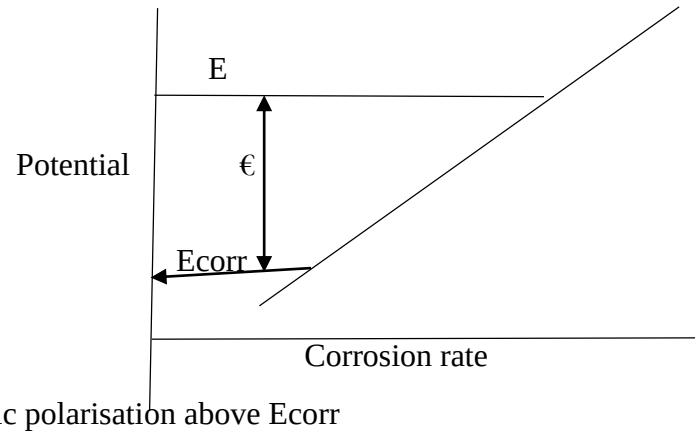

Fig 2.2 Anodic polarisation above Ecorr

2.2.2 Passivity

Anodic polarization, not in every case results in the increase in the corrosion rate. In metals like iron, chromium, titanium and cobalt, the corrosion rate decreases with the application of anodic polarisation. There exist a critical potential Epp above which there is a drastic fall in corrosion rate in spite of higher driving force i.e. anodic polarisation as shown in Fig 2.3 resulting in formation of a thin passive layer [12]. This phenomena is defined as passivity. Below Epp the rate of dissolution is relatively high. There is a reduction of 10^3 to 10^6 times in corrosion rate while transiting from the active region to passive region rendering very low dissolution rate in passivation state. In the passive region the current remains almost constant even with increasing anodic polarisation. This can be attributed to the development of a very thin, adherent, stable oxide layer on the surface of the metal that prevents the underlying metal to come in direct contact with the atmosphere and subsidise the effect of anodic polarisation.

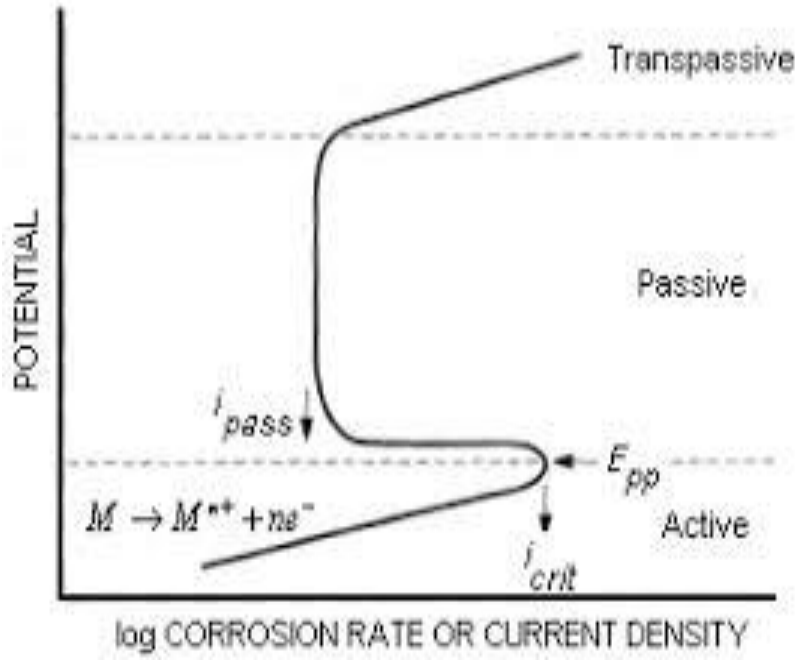

Fig 2.3 Passivity at oxidizing potential above Epp

The metal/alloy can exist in active or passive state depending on the oxidizing power of the solution and the polarizibility. Type 304 stainless steel is passive in aerated but active in deaerated salt water.

Chromium is one of the main ingredient in most of the alloys for achieving passivation. Stainless steel contains about 12.5 % chromium, which imparts excellent corrosion resistance. Other combinations of Nickel and chromium are used in high temperature application, electrical appliances etc.

As already stated passivity is the formation of thin oxide layer, this layer is fragile and susceptible to breakdown. The breakdown of the passive layer can results in unpredictable localised forms of corrosion like pitting, crevice and embrittlement to be discussed in the next section.

2.3 Forms of corrosion

Various forms of corrosion are listed below and schematic description as shown in Fig 2.4.

- Uniform corrosion
- Galvanic corrosion
- Crevice corrosion
- Pitting corrosion
- Environmentally induced corrosion
- Hydrogen damage
- Intergranular corrosion
- Dealloying
- Erosion corrosion

Uniform Corrosion

Galvanic Corrosion

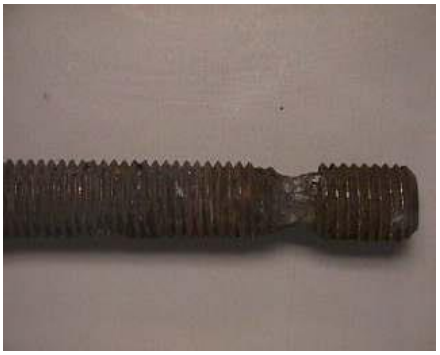

Crevice Corrosion

Pitting Corrosion

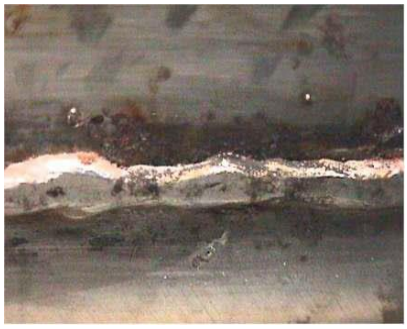

Intergranular Corrosion

Selective leaching/
Dealloying

Cavitation

Hydrogen cracking

Uniform Corrosion

Fig 2.4 Schematic summary of the various from of corrosion

2.4 Pitting Corrosion

Pitting corrosion is the localised formation of small pits which are not easily seen by naked eyes as they are easily hidden by inoffensive corrosion products surrounding its periphery, results in relatively rapid penetration. This kind of corrosion is usually unpredictable and insidious and hence can result in catastrophic destruction. Stainless steel used in marine and chemical industries are seen to have undergone prominent pitting corrosion. The important requirement for pitting to occur is the presence of aggressive chloride ions in neutral to acid solution.

2.4.1 Mechanism of pitting corrosion

Pitting corrosion is usually catalytic in nature. Once started the process has the ability to sustain itself given the environmental conditions remain the same. The differential aerated model as explained by Evans water drop experiment can help explain the mechanism of pitting corrosion [8]. Shown in Fig 2.5 is the pitting of a metal M in an aerated sodium chloride solution.

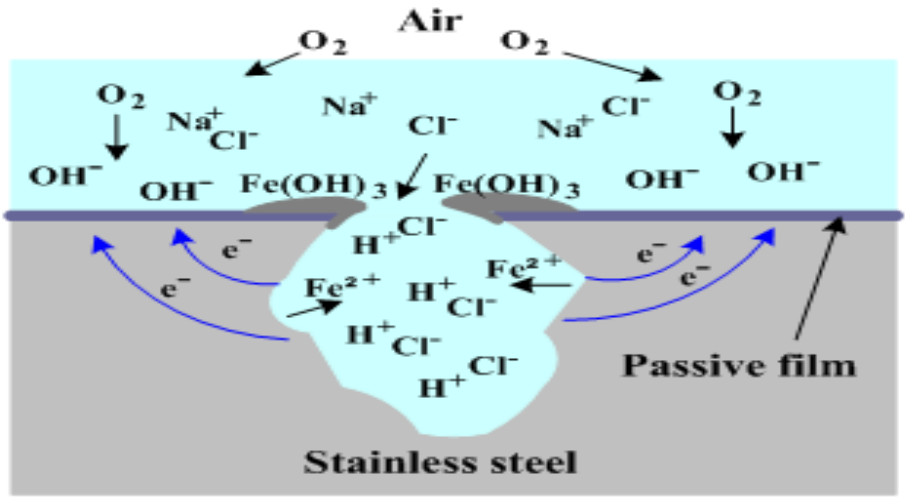

Fig 2.5 Mechanism of Pitting corrosion

While the inside of the pit is anodic, the external surface near to the pit act as cathode. The inside of the pit is positively charged because of the rapid dissolution of the metals, which attract negatively charged chloride ions to the pit maintaining electro neutrality. This chloride ions reacts with the metal to from MCl inside the pit, which results in localised decrease in pH which is highly simulating for more and more metal dissolution. The pit provide a safe and sheltered area that prevents easy mass transport between the pit and the exterior bulk solutions. The solubility of the oxygen is negligible in concentrated solutions, and hence no reduction of oxygen takes place inside the pit. The above figure clears explain on how the pit sustains itself but gives no idea on how the process is initiated. Pitting initiates when the potential exceeds a critical pitting potential, Epit, which is used to measure the resistance to pitting corrosion. Higher is the value of Epit, the more is the resistance to pitting corrosion and vice versa. The presence of chloride ions results in an increase in the anodic currents at all higher potential as shown in Fig 2.6. But the most important output of the presence of the chloride ions is the decrease in the value of Epit. Any anodic polarization above Epit leads to immediate increase in the flow of current, this potential signifies the localised rupture of the protective film on the surface of the metal [9].

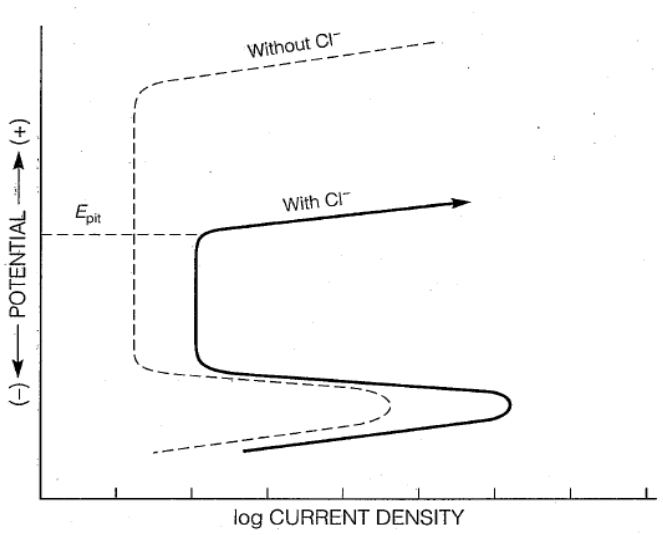

Fig 2.6 Initiation of Pitting above Epit

Once the film is ruptured, and corrosion products are formed effective mass transfer and chemical reactions can't take place between the bulk solution and the underlying metal as explained above. The corrosion products formed gets deposited on the tip of the pit and prevents flow of mass which helps in accelerating the rate of dissolution inside the pit. Once the pit is formed, it can continue growing inside to from a crack. The conditions should be established for successful growth of the pit. If these conditions are not achieved the pit growth will stop [10]. There are various parameter defined to determine if an alloy is susceptible to pitting corrosion depending on the composition of the alloy. Fig 2.7 shows the initiation, propagation and growth of pits on iron by the localised breakdown of the external protective passive layer[11]. The protective layer here is FeOOH which gets dissolute to from soluble FeOCl salt Island which rapidly dissolute to expose the underlying metal and formation of pits [9]. Fig 2.8 is a cartoon representation of the various stages of pitting corrosion.

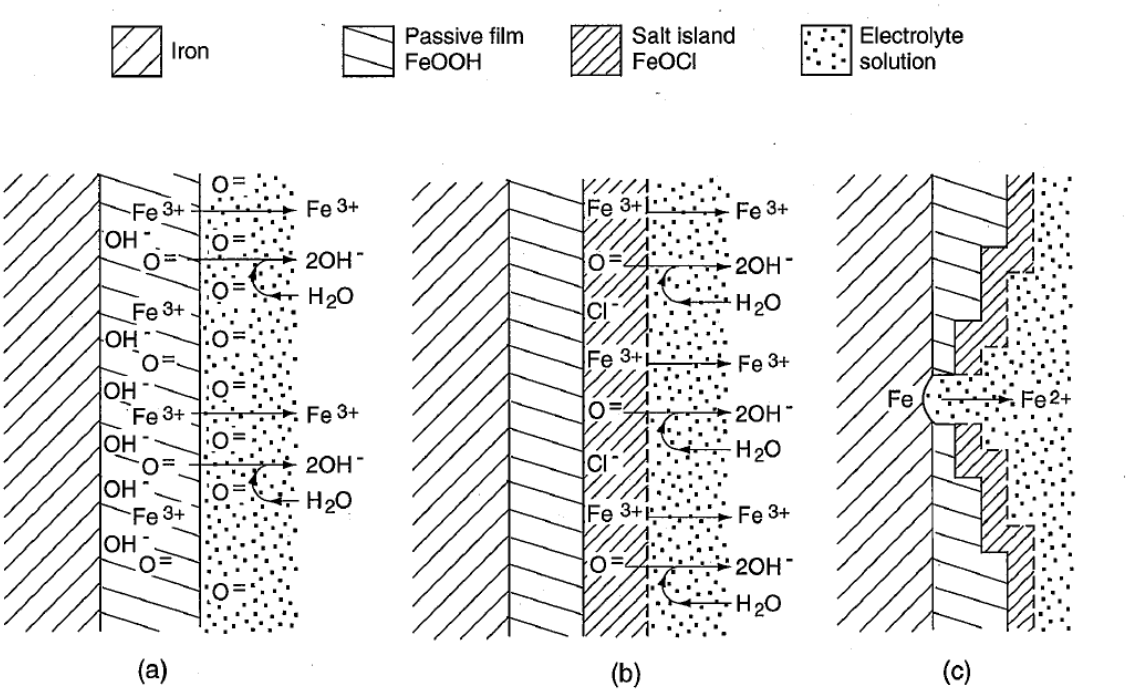

Fig 2.7 Pitting of Iron. (a) Initiation by dissolution of passive film, (b) accelerated dissolution at a soluble salt island, (c) Formations of pits by direct anodic dissolution

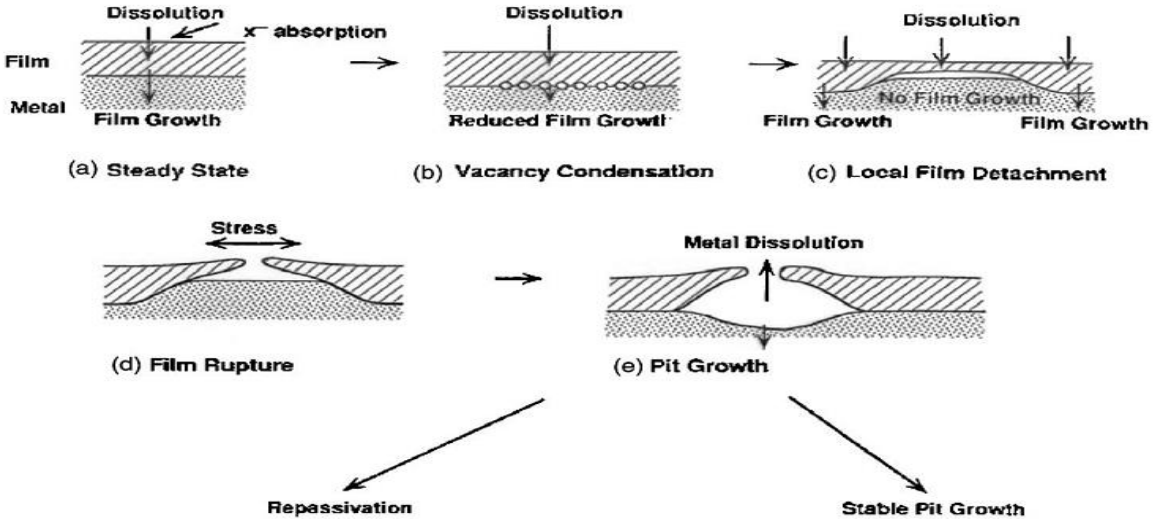

Fig 2.8 Cartoon representation of the stages of pitting corrosion

2.5 Passivity and Passivity breakdown- Modelling

The initial events in the accumulation of the localised corrosion damage (LCD) are passivity breakdown and pit nucleation, which readily occur in the severely corrosion environments containing concentrated chloride. Subsequently, the pits that grows to critical dimensions act as sites for the nucleation of cracks. Therefore, passivity breakdown and pit nucleation on the carbon steels are of great importance in relevance to the risk associated with the operation of various important industries which serves the basic requirement of our sustenance. The point defect model (PDM) provides a deterministic description of passivity breakdown [13] on metals and alloys. Previously all characterisation of passivity was based on analytical observation but with the development of modelistic approach, the stability and characterisation of the passivity and its breakdown can be well assessed, following which a comparison between the two can be made and the validity of the model can be estimated.

2.5.1 Inception and development

As stated, Passivity is the formation of a 3 dimensional oxide layer which protects the surface of the metal. Since the discovery of passivity, various laws and equations were described to account for the growth of the passive layer, and finally, the growth kinetics was attributed to the following laws where experimentally data shows both having equal credibility [14]

$L = A + B \ln t$ (logarithmic law)

$1/L = C - D \ln t$ (Inverse logarithmic law)

Where A, B, C, D are constant, L and t stands for thickness and time respectively.

Since the applications of modelling in experimentally analysis, several models were discovered to attribute the above laws. We will now discuss some of the models developed and their shortcomings.

Mott- Cabrera Model – Developed in 1947, this is one of the earliest model developed to account for growth kinetics of passive films. It was proposed by Mott [15] in 1947 and was modified by Cabrera and Mott (16) in 1948. The basic assumption of this model are:

(i) The transfer of the metal cations across the oxide layer to the film/solution interface, wherein it react with the electrolyte is the basis of the film growth kinetics.

(ii) The high electric field strength present in the oxide layer is responsible for the injection and transfer of cations across the film.

(iii) The field strength is constant throughout the film

(iv) The emission of metal cations from the metal into the film at the metal/film interface is assumed to be the rate limiting step.

These assumptions shows that the film growth kinetics follows the inverse logarithmic law.

Sato and Cohen's model - Study of iron in pH 8.4 borate buffer solution, Sato and Cohen [17] found the dependence of the external current, i, the applied potential, Vapp, and the accumulated charge in the oxide film, QT.

$$i = k' \exp (mVapp -- QT/n)$$

Where k', m, and n are parameters.

This model was then explained using the terms "place-exchange" mechanism by the author to explain their results. According to this model, a layer of oxygen is adsorbed onto the surface which then exchanges places (possibly by rotation) with underlying metal atoms. A second layer of oxygen is then adsorbed and the two M-O pairs rotate simultaneously. A schematic representation of this mechanism is shown in Fig. 2.9.

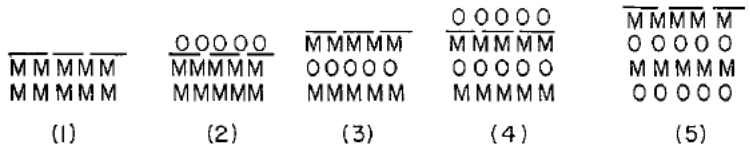

Fig 2.9 Oxide film growth by the "place-exchange" mechanism. M and 0 represent metal and oxygen atoms, respectively. The dashed line is the solid-electrolyte interface. (1) A film-free metal; (2) oxygen adsorption on the metal surface; (3) "place-exchange" between oxygen and metal; (4) second oxygen layer is adsorbed; (5) "place-exchange" between two M-O pairs

Fehlner and Mott's model – in 1960, Eley and Wilkinson [18] found out that the logarithmic growth law could be obtained by assuming any mechanism whose activation energy increased linearly with film thickness. Based on this argument, the "place-exchange" model was given importance, since this model assumes linear dependence of film thickness on activation energy. Further work was done by Sato and Cohen for several years to develop this model.

All the models cited above couldn't explain various fundamental aspects of the experiments, neither did they fall in well agreement with the experimental data. None of the model could explain the potentiostatic transients obtained during the film growth kinetics of iron in sodium hydroxide solution [19]. The inverse logarithmic law is followed when the pH is low, the Mott Cabrera model didn't take this into significance. The anionic transportation also plays an important role in the film growth kinetics which was not addressed by the model.

In 1981, a new model called the Point defect model was presented to account for the film growth kinetics and the passivity breakdown. Subsequently, it was found that this model satisfactorily aligned itself with the various experimental data from the literature.

2.5.2 Point defect model

The newly developed Point defect model is based on the following assumptions [19-24]:

(i) The external potential Vext, whenever exceeds the flade potential, a continuous thin and adherent film is formed on the surface of the metal. As per the model, the film is assumed to be a oxide film, $MO_{x/2}$, but the model is affectively applicable for films other than oxide such as hydroxides.

(ii) The passive film is assumed to be a sea of point defects. The major point defects that exist in an oxide film are V_M, Vo", e', and h'*. The same species are expected to be present in a passive film.

(iii) High electrical fields of the order of 10^6 V/cm are seen in the passive films and this high electrical field is sufficient for keeping the film on the verge of electrical breakdown. Hence, the passive film behaves as an "incipient semiconductor" because it exists on the verge of dielectric breakdown. The field strength is a function of the chemical and electrical characteristics of the film and therefore is independent of thickness even for potentiostatic conditions.

(iv) Since passive films are regarded to be "incipient semiconductors," it is assumed that electrons (e') and electron holes (h') in the film matrix are in their equilibrium states, and that the electrochemical reactions involving electrons (or electron holes) are rate controlled at either the metal/film (m/f) or the film/solution (f/s) interfaces. On the other hand, the rate controlling step for those processes which involve metal vacancies (Vm) and oxide vacancies (Vo"), (i.e., film growth) is assumed to be the transport of the vacancies across the film. This assumption implies that metal and oxide vacancies are in their equilibrium states at the m/f and the f/s interfaces.

The point defect proposes that the movement of anionic vacancy and cationic vacancy generated at film/barrier and metal/film interface respectively and the flux generated by these vacancies movement are responsible for the formation of the passive layer and also its breakdown.

*The Kroger-Vink notation is adopted here for designating point defect species. According to the notation, X~ means that a species X occupies a u lattice site (e.g., V~ means a vacancy occupies a metal site in the oxide, i.e., a metal vacancy); e and h are electrons and holes. The superscript gives the number and the sign of the charge. Thus, ", ." means two positive charges."X"" means x negative charges (e,g. V~tx' means a metal vacancy which carries X negative charge).

2.5.2.1 Passivity

The study of the formation and stability of the passive film is of paramount importance as the thickness of the passive film should be as large as possible. As already mentioned the passive film is a semiconductor device, the nature of the film, whether it is p-type or n-type, also plays equally important role. Various experimental techniques like Mott schottky analysis and electrical impedance spectroscopy can give information about the nature and thickness of the film. N-type films are those in which anionic vacancies and interstitials plays important role while in p type films, cationic vacancies movement results in film formation. While the film can behave both as n and p-type depending on the external potential. The point defect effectively proves that the growth of the film follows either logarithmic or inverse logarithmic law. According to the model, diffusion of anionic vacancies results in film growth while the same for cationic vacancies result in metal dissolution. The schematics of the various reactions taking place at the m/f and f/b interface is shown in figure 2.10.The Generation I Point defect model doesn't take into consideration the effect of interstitials as a result of which various errors results in when compared with the experimental data. PDM-I failed ultimately, because it could not account for the existence of the commonly observed steady-states in passive current density and barrier layer thickness. It also became apparent that, in many cases, where the film is n-type, there must be a mobile donor other than the oxygen vacancy that can account for the current. That species was subsequently identified as the cation interstitial. Finally, PDM-I did not distinguish between reactions as to their lattice conservation nature and it did not recognize the formation of the outer layer. This led to the development of PDM-II in the early 1990s.

The Lss, thickness of the film, is dependent of the applied potential. As the anodic polarisation increase in the positive direction the thickness of the film increases as is clearly evident from the anodic polarisation curve. The value of Iss remain quite independent of the applied potential. Various experiments which incorporate point defect model to account for the passivity verified the above phenomena.

$$L_{ss} = \frac{1}{\varepsilon}\left[1 - \alpha - \frac{\alpha\alpha_7}{\alpha_3}\left(\frac{\delta}{X} - 1\right)\right]V + \frac{1}{\varepsilon}\left\{\frac{2.3.0n}{\alpha_3 XY} - \beta\left[\frac{\alpha_7}{\alpha_3}\left(\frac{\delta}{X} - 1\right) + 1\right]\right\}pH + \frac{1}{\alpha_{3XK}}\ln\left(\frac{K_3^0}{K_7^0}\right) \quad (1)$$

$$I_{ss} = \delta F\left[K_2^0 e^{a2V} e^{b2Lss} e^{c2pH} + K_4^0 e^{a4V} e^{c4pH} + K_7^0 e^{a7V} e^{c7pH}.\left(\frac{C_{H+}}{C_{H+}^0}\right)^n\right] \quad (2)$$

Where Lss is the thickness of the film, Iss is the passivation current density, ε is the relative permittivity of the passive film, α is the polarizabilty, α_s is the diffusion factor where s represents the equation number in Generation II model, k_s stand for the rate constant of the equation, n stands for number of electrons, x and δ are the oxidation states in film and solution respectively.

2.5.2.2 Passivity breakdown

The point defect model proposes that cation vacancies ($V_M^{x\prime}$) generated at the film/ solution interface move to the metal/film interface as shown in Fig 2.10, and are annihilated by cation injection into the film from the metal [19-21]

$$m + V_M^{x\prime} \rightarrow M_m + v_m + xe' \quad (3)$$

Where m and v_m are a metal atom and a metal vacancy in the metal phase, respectively; $V_M^{x\prime}$ and M_m are a cation vacancy and a cation in normal cation sites on the cation sub lattice of the barrier layer. The annihilation rate of the cation vacancies ($V_M^{x\prime}$) at the metal/ film interface is depicted as J_m. Aggressive anion absorption (e.g.: chloride anion) into surface oxygen vacancies ($V_o^{\blacksquare\blacksquare}$) catalyzes the generation of cation vacancies possibly via a schottky-pair reaction or anion-assisted cation extraction and leads to an enhanced flux of the cation vacancies (J_{ca}) toward the metal/film interface. The cation vacancies condense at the metal/film interface if J_{ca} exceeds J_m ; furthermore, when the areal concentration in the condensate excess a critical value(ξ), local separation of the barrier layer from the substrate metal occurs. This local separation process continues at the periphery of the condensate causing the condensate to expand and preventing the film from penetrating into the substrate via the generation of oxygen vacancies via

$$m \rightarrow M_m + \frac{x}{2} V_o^{\blacksquare\blacksquare} + xe' \quad (4)$$

However, dissolution continues at the outer surface with the result that the barrier layer over the condensate thins at a rate that is determined by the dissolution rate and, at some point, the "cap" (remnants of the barrier layer) over the condensate will rupture to mark passivity breakdown event. The critical concentrations of cation vacancies that must condense per unit are (ξ) for separation to occur between the barrier layer and the metal substrate is determined

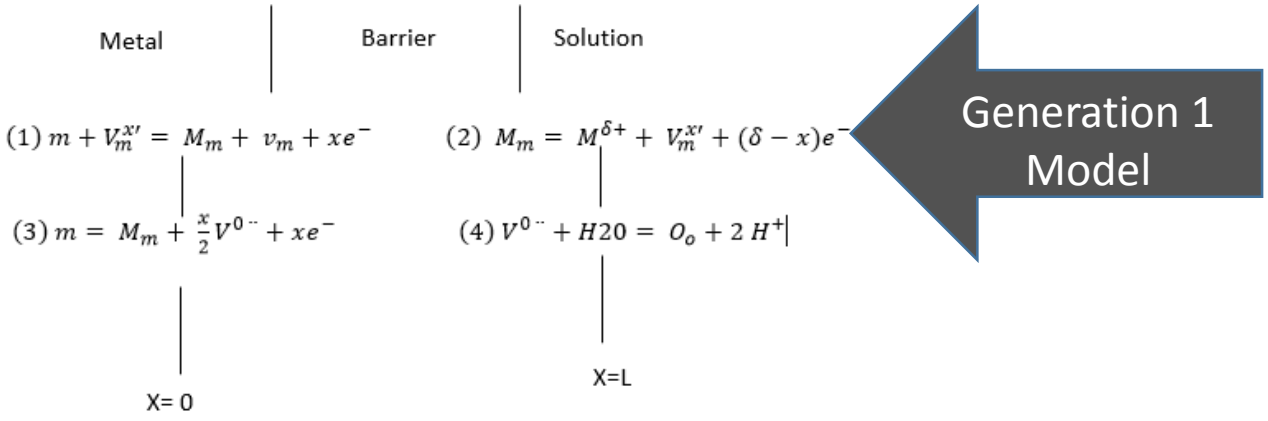

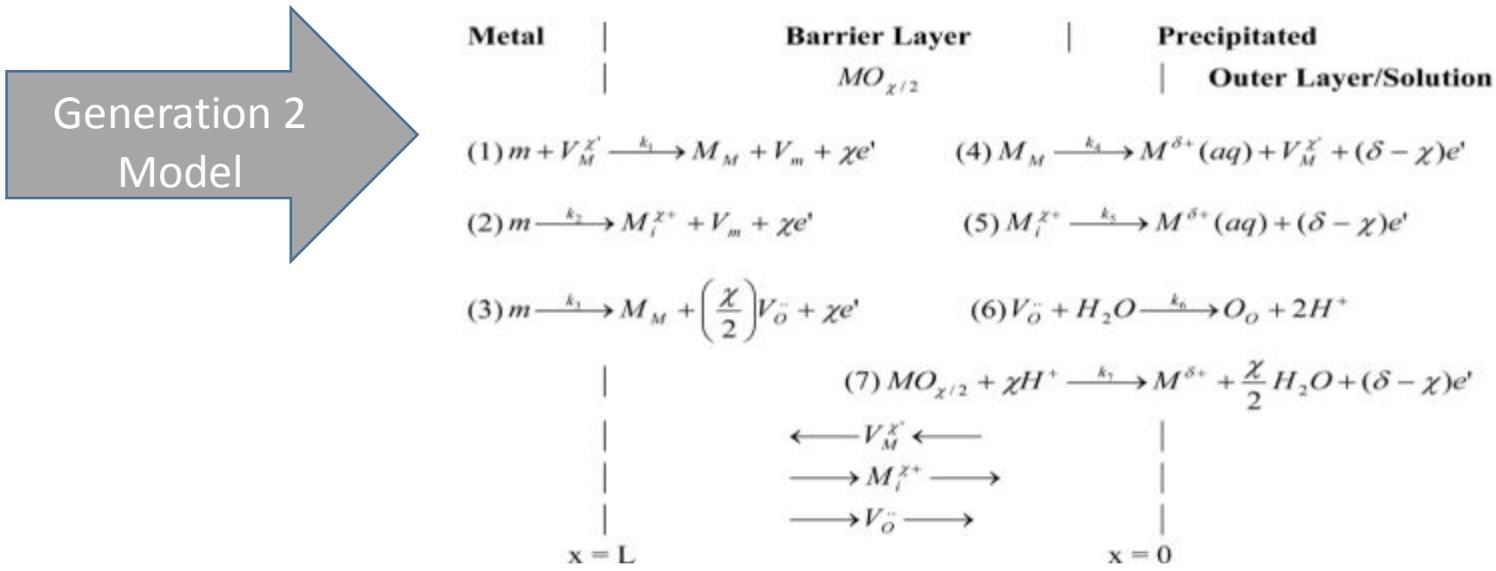

Fig 2.10 Generation 1 and Generation 2 of the Point defect model

by the structures of the metal and the film, depending on whether condensation is envisioned to occur on the metal lattice or on the cation sub lattice of the film. Fig 2.11 summarises the set of equations defined by the point defect model. As, the first generation couldn't account for all the observation, generation to was developed with added equations to account for the errors.

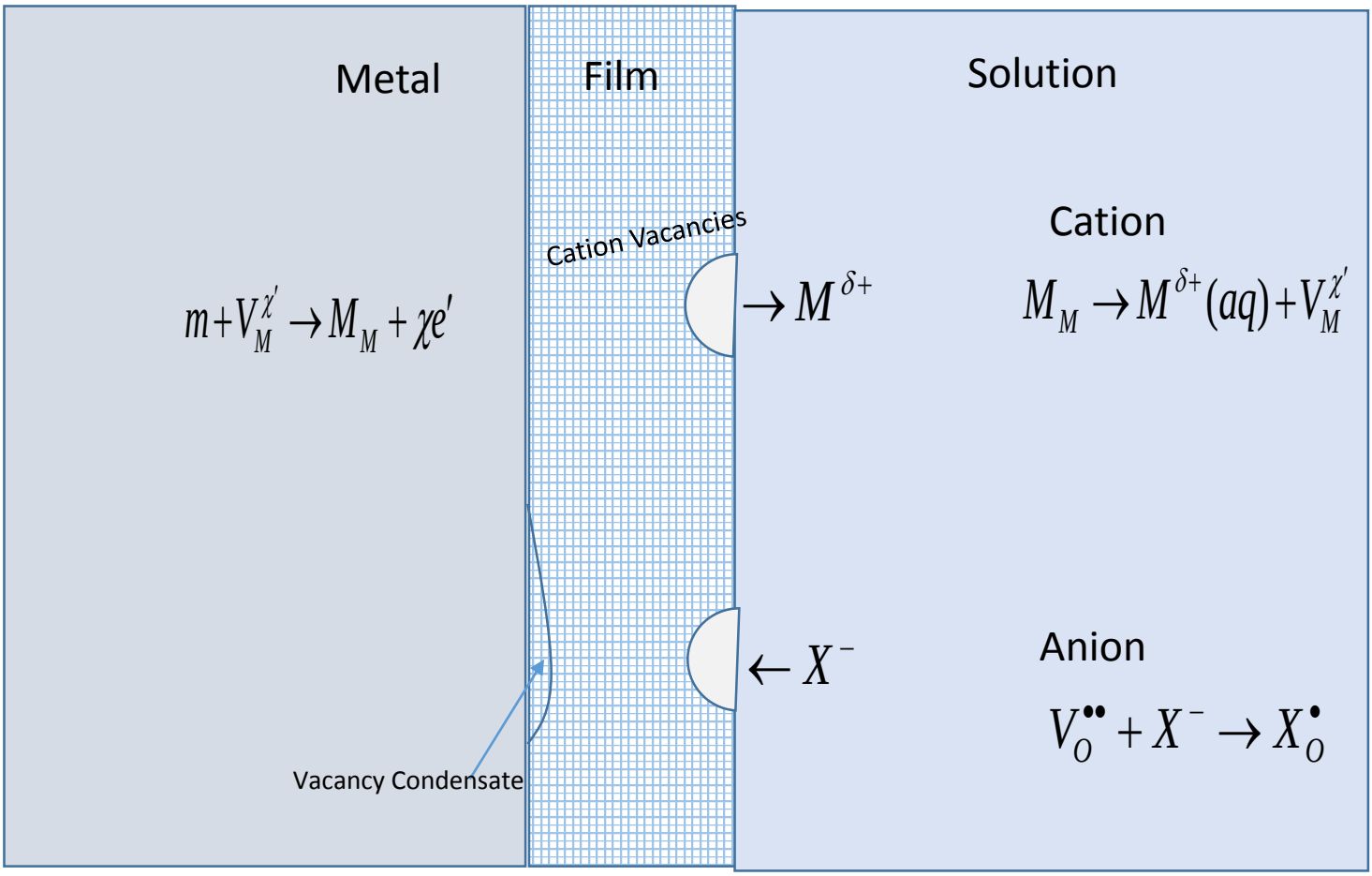

2.11 Process leading to the breakdown of passive films according to the PDM

According to this mechanism, taking into account only chloride ion adsorption schottky-pair vacancy generation, the following relationship for the critical breakdown potential (V_c) was derived

$$V_c = \frac{4.606RT}{\chi\alpha F}\log\left(\frac{b}{D}\right) - \frac{2.303RT}{\alpha F}\log\left(a_{Cl^-}\right) \quad (5)$$

Where

$$b = \frac{RTJ_m\Omega}{F\chi\varepsilon N_V} \times \exp\left(\frac{\Delta G_s^0 + \frac{\chi}{2}\Delta G_A^0 - \frac{\chi}{2}\beta FpH - \frac{\chi}{2}F\phi_{f/s}^0}{RT}\right) \quad (6)$$

$$\phi_{f/s} = \phi_{f/s}^0 + \alpha V + \beta \mathrm{pH} \quad (7)$$

It can be easily concluded from equation 5, that the breakdown potential, Vc, decreases with the increasing chloride concentration and vice versa. The slope of this curve gives the value the polarazibilty constant, α. The dependence of pH can also be determined from the equation. With the increase in the pH, the breakdown potential also increase, and the slope of this curve gives the value of β, the dependence of the film/solution interface potential on pH.

Passivity breakdown in envisioned to occur at sites on the surface that are characterized by high cation vacancy diffusivity. These site are considered to include the regions of high disorder in the structure of the barrier layer that might exist, for example, at points of intersection of the barrier layer with inclusions. The potential breakdown sites are assumed to be distributed normally with respect to the cation vacancy diffusivity with the distribution characterized by a mean value, $\overline{D}$, and a standard deviation σ_D [23], Based on this postulate, an analytical distribution function for V_c is readily derived as Eq. (8). Importantly, V_c is predicted to follow a near normal distribution, as has been observed experimentally

$$\frac{dN}{dV_c} = \frac{-b\gamma'}{\sqrt{2\pi}.\sigma_D.a_{Cl^-}^{\chi/2}} \exp\left[\frac{-\left(e^{-\gamma' V_c} - e^{-\gamma' \bar{V}_c}\right)^2 b^2}{2\sigma_D^2 a_{Cl^-}^{\chi}}\right] \exp\left(-\gamma' V_c\right) \quad (8)$$

Where,

$$\gamma' = \frac{\chi\alpha F}{2RT} \qquad \bar{V}_c = \frac{1}{\gamma'} Ln\left(\frac{b}{D} \times a_{Cl^-}^{-\chi/2}\right)$$

The cumulative probability in breakdown potential is defined as Eq. (9), where P (V_c) represents the percentage breakdown sites at Vc in all possible breakdown sites

$$P(V_c) = 100 \times \frac{\int_{-\infty}^{V_c}\left(\frac{dN}{dV_c}\right)dV_c}{\int_{-\infty}^{\infty}\left(\frac{dN}{dV_c}\right)dV_c} \quad (9)$$

2.6 Summary

Pitting corrosion is one of the most prominent form of corrosion occurs in the presence of aggressive chloride ions by passivity breakdown. The characterisation of passivity breakdown has been addressed since years by development of various models, among which Point defect model was able to clearly explain the phenomena of passivity and passivity breakdown while addressing film growth kinetics. The point defect model also is the only model that satisfactorily falls in well agreement with the experimentally obtained data for the study of passivity and its breakdown. The model is still undergoing changes to also account for the passivity on alloy.

Chapter 3

Experimental details

Polished samples of high manganese carbon steel was prepared and passivity breakdown studies of the same was studied at different concentration of chloride ions in borate buffer, varying pH at potential scan rate. The experimental set up to study the same along with the preparation of the borate buffer has been described in this section.

3.1 Sample preparation

High manganese carbon steel, composition of which is given in Table 3.1, is a low carbon, high manganese steel used extensively in pressure vessels. The very high concentration of manganese provide the important property which makes this metal useful for bearing high pressure.

3.1.1. Grinding and polishing:

High manganese carbon steels specimens were cut from a commercial round bar (diameter d=1.2cm). The specimens were first polished on a metal grinder to get a flat and smooth surface. It was followed by mechanically grounding the specimen with emery paper of grit 240/400/600/800 and 1200 for about 10 minutes on each of the emery paper and rotating 90 degree after moving from one paper to another. Finally the specimens were polished on diamond polisher until a mirror finished was obtained with little or no scratch. This was a wet polishing as water was continuously supplied.

Table 3.1: Composition of high manganese carbon steel

C	Mn	P	S	Si	Cu	Ni	Cr	Mo	Al
0.15	0.980	0.005	0.0005	0.324	0.043	0.059	0.082	0.009	0.034

3.1.2 Cold mounting

The prepared specimens were then taken to the Central Workshop where threading was done on the back side of the sample for the insertion of the copper wire. The specimens were then cold mounted in an epoxy resin containing about 10% hardener for about 24 hours. After that the plastics used to cold mounting were ripped off to provide the final sample. Care was taken to avoid scratching of the surface. The working surface area was 1.27 cm^2.

3.2 Borate buffer preparation

During pitting corrosion there are chances of localised changes in pH which can be avoided by using borate buffer. Borate buffer of different pH and chloride concentration were prepared for this study.

Boric acid and sodium pellets were used to balance the pH of the solution at different chloride concentration as shown in Table 3.2. The chloride concentration was varied at a constant pH of 10.04. This was arranged by adjusting the boric acid composition in the solution.

Table 3.2: Composition, measured pH, of borate buffer solutions containing different concentrations of sodium chloride

Solution Composition	**pH**
0.75M H3BO3 + 0.020M NaOH + 1 M NaCl	**5.9**
0.50M H3BO3 + 0.25M NaOH + 1 M NaCl	**8.2**
0.50M H3BO3 + 0.4M NaOH + 1 M NaCl	**9.04**
0.45M H3BO3 + 0.5M NaOH + 1 M NaCl	**10.02**
0.60M H3BO3 + 0.5M NaOH + 0.01 M NaCl	**10.02**
0.55M H3BO3 + 0.5M NaOH + 0.1M NaCl	**10.02**
0.50M H3BO3 + 0.5M NaOH + 0.6 M NaCl	**10.02**

3.3 Electrochemical setup

All electrochemical measurements were conducted in a single compartment glass cell using a Autolab Potentiostat. The schematics of the electrochemical setup is shown in Fig 3.1. The high manganese carbon sample was dipped in the electrolyte as shown in the figure below. The counter electrode was a Pt wire sealed in a glass that was house in a separate glass tube with a porous glass frit. The reference was an Ag/AgCl electrode that was housed in a Luggin capillary with a cracked glass tip. The working electrode was a polished surface of high manganese carbon steel. All experiments are carried out at room temperature. The connections were all colour coded and same was maintained for almost every experimental analysis

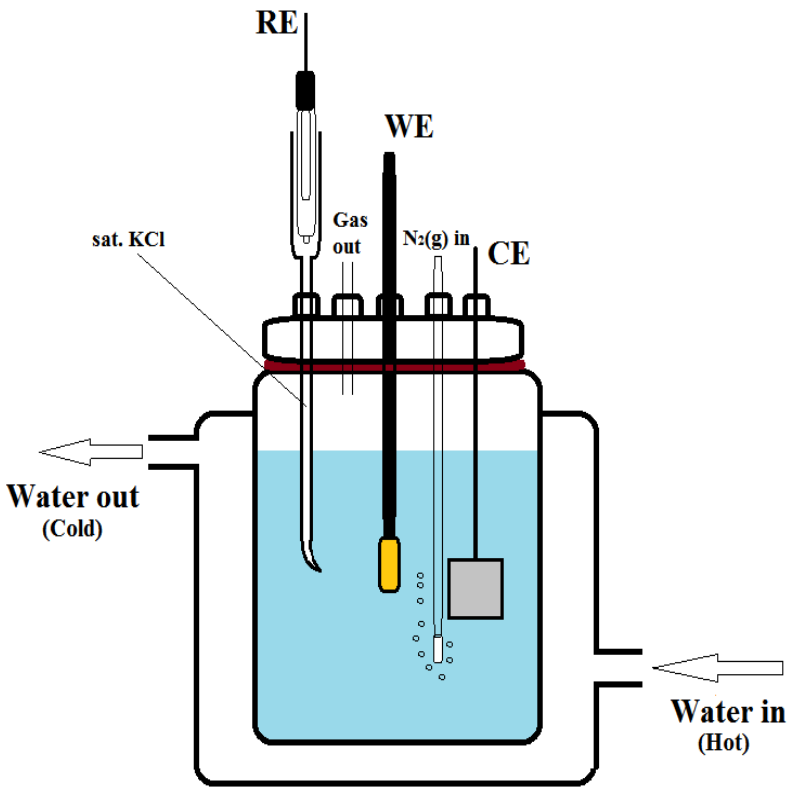

Fig 3.1 Schematics of the electrochemical setup

3.4 Electrochemical Measurements

Various potentiodynamic plots were plotted to find out the various process parameters to account for the modelling part in reference to Point defect model. The passivity is studied by plotting the potentiodynamic curves and selecting five potential at which passive films were formed and electrical impedance spectroscopy assuming Randles circuit as shown below was done to study the capacitive and resistive nature of the films followed by Mott Schottky analysis to find the defect type whether p- type or n type. Then calculations were done for Lss and Iss using point defect model. .

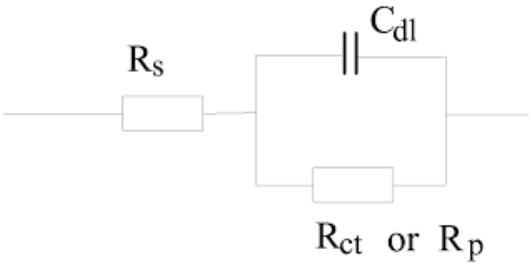

Firstly, V-I plots were plotted for different chloride concentration a_{cl}^- [0.01, 0.1, 0.6, 1 M]. From this data a curve in between Vc and a_{cl}^- was plotted which gave the value of α. Secondly, the potentiodynamic scans were done at different scan rate, *v*, whose Vc vs *v* slope gave the value of the critical area concentration for passivity breakdown. The various scan rate used were 0.1, 0.4, 2.5, 5 10 mV/seconds. Potentiodynamic plots were then plotted for 20 times for finding the cumulative probability distribution of breakdown potential at different pH [5.9, 8.2, 9.04, and 10.02]. The cumulative probability distributions of breakdown potential obtained experimentally was then compared with the modelling one to account the validity of Point defect model. Potentiodynamic plots obtained at different pH were also used to give the value of β.

Chapter 4

Results and discussion

This chapter summarises the various potentiodynamic curves obtained from the experimental data, and helps in deriving the process parameters in accordance to the Point defect model for the computational modelling of the passivity breakdown studies. The modelling when superimposed with the experimental data, concludes well alignment between each other.

4.1 Passivity studies on high manganese carbon steel

The potentiodynamic curve was plotted at a very low scan rate of 0.1 mV/ sec to obtain the cathodic and anodic polarisation data as shown in figure 4.2. The figure shows a well-defined passive regions in the range of -0.3 V to 0.8 V. Five potential, -50, 100, 250, 400, 550 mV, in this range were chosen to study the passive film on this grade of steel.

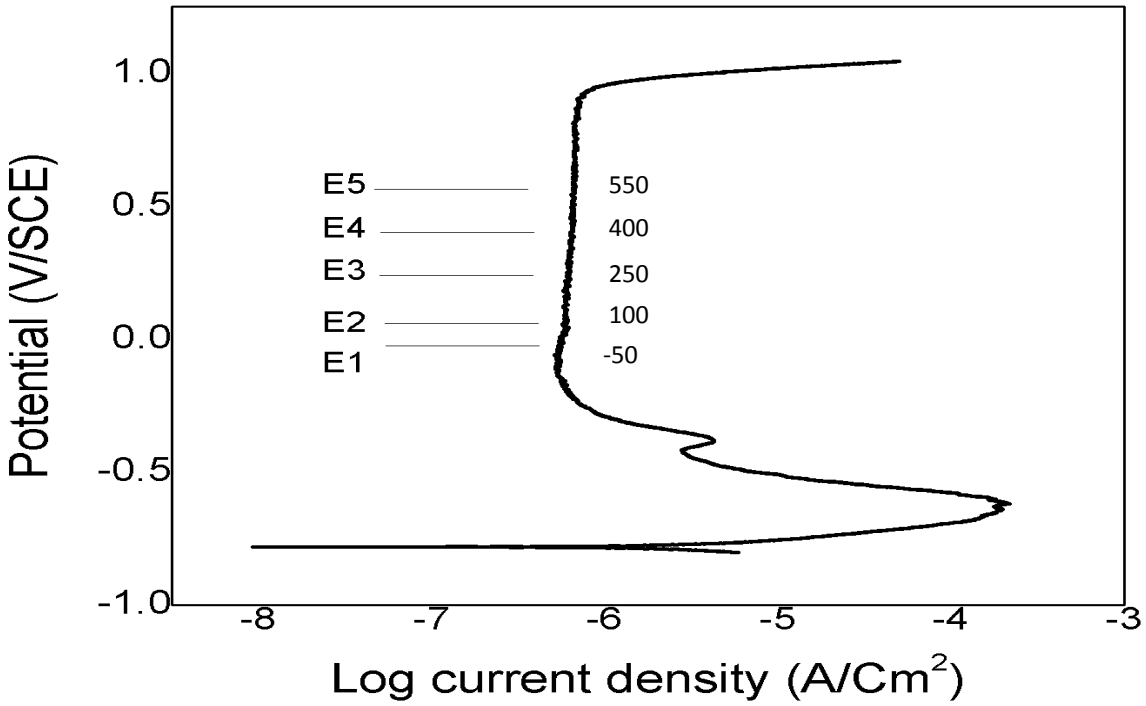

Figure 4.1: Potentiodynamic polarization curves (υ = 0.1667 mV/s) for type high manganese carbon steel in deaerated borate buffer solutions

The solution prepared was having a pH=8.2 without any chloride concentration. Figure 4.2 shows the OCP for five samples prepared. The OCP for this grade of steel in pH=8.2 was found to be 0.75 V. The OCP was run for 1800 seconds. Initially the potential was found to be unstable until 400 seconds, henceforth which it was stable.

4.1.1 Mott Schottky Analysis

The Mott Schottky analysis was done for all the above potential to study if any changes occurs in the type of defect. Basically, Mott Schottky analysis is a plot between $1/C^2$ and potential V related by the following equation:

$$\frac{1}{C^2} = \pm \frac{2}{\varepsilon\, \varepsilon_o e N}(V + c) \qquad (10)$$

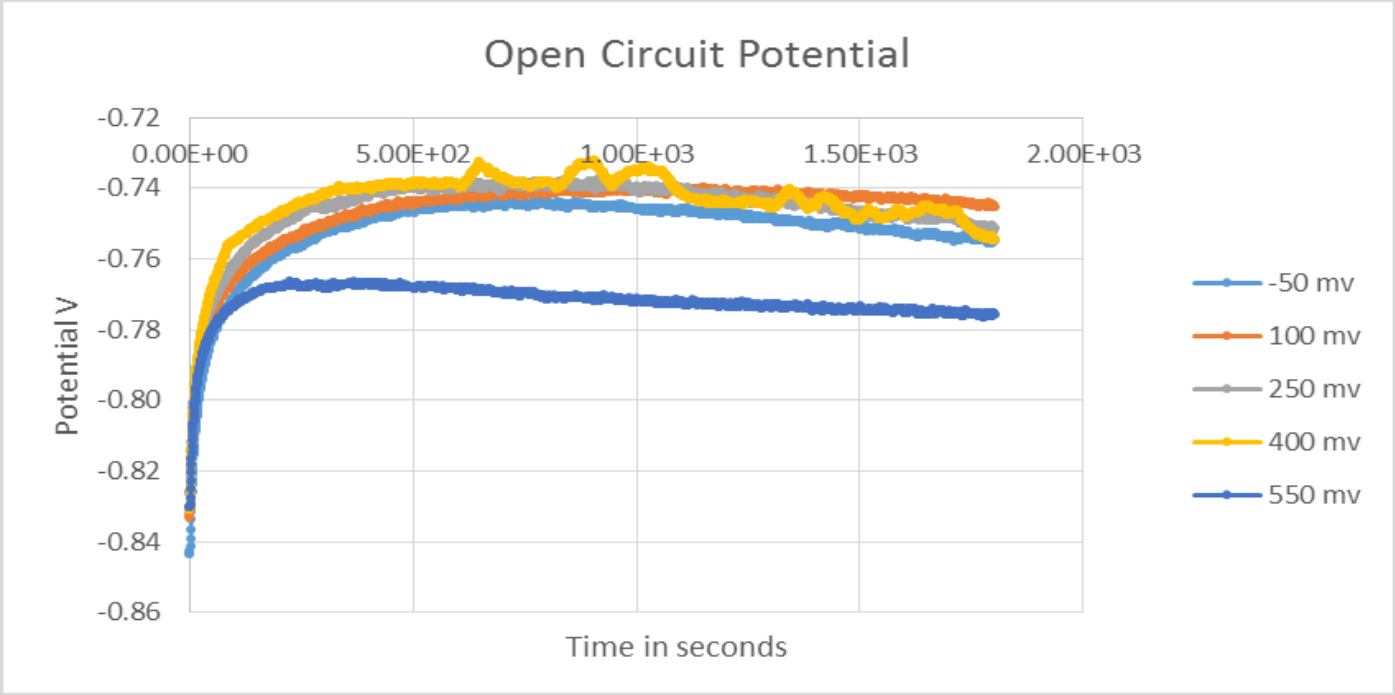

Figure 4.2: Open circuit potential for type high manganese carbon steel in deaerated borate buffer solutions.

Where C is the capacitance, N is the donor concentration and c is some constant. A positive slope in the above equation signifies n-type defects while a negative slope signifies p-type defect film. While both defects can be seen in the analysis depending on the applied potential. The Mott Schottky analysis of the high manganese carbon steel is shown in figure 4.3. The analysis shows n type behavior till -400 mV as the slope is positive and then the slope turns negative and the film behaves as a p-type defect structure.

From the slope of the curve in Figure 4.3, the donor concentration for various passivation potential can be found. Figure 4.4 shows the curve for Donor concentration vs. potential, which clearly shoes the done concentration is almost independent of the passivation potential.

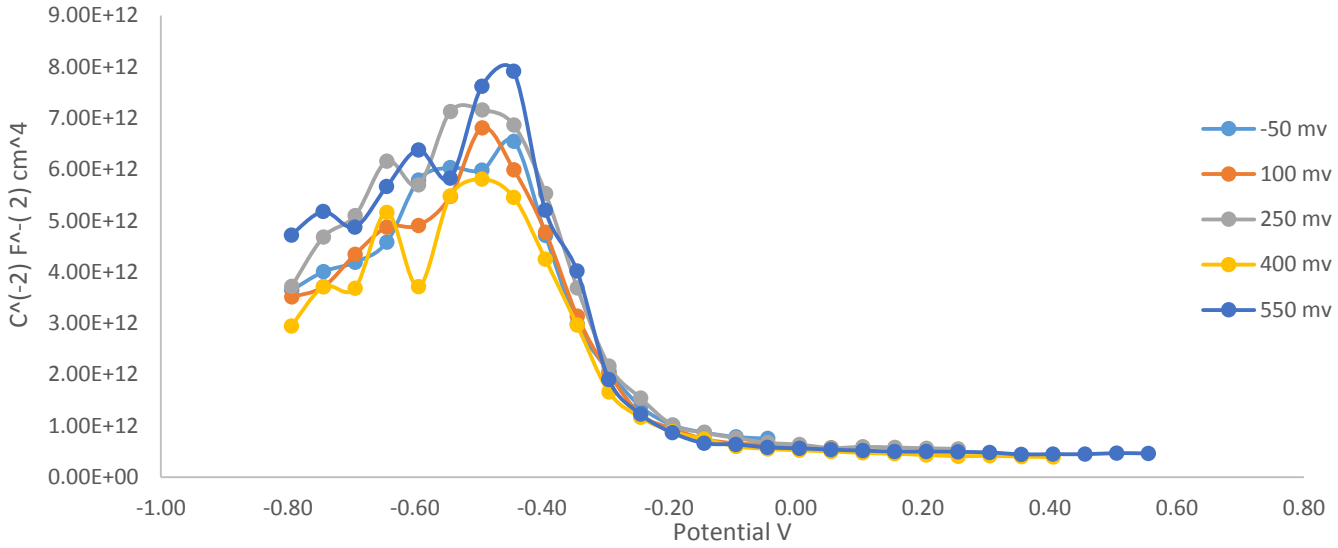

Figure 4.3 Mott Schottky analysis of the passive layer at different passivation potential

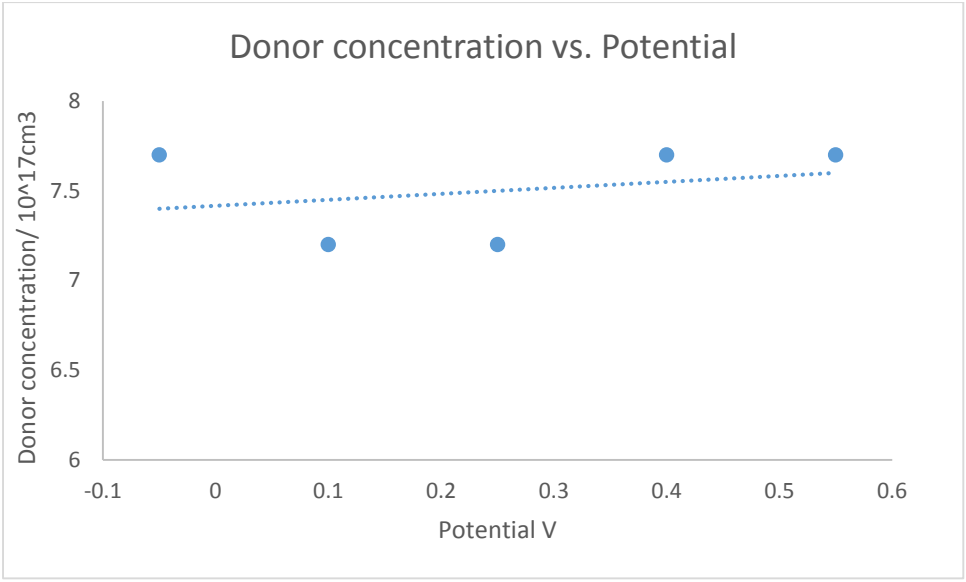

Figure 4.4: Donor concentration vs. Potential obtained from the slope of the curve of Mott Schottky analysis

4.1.2 Electrical Impedance spectroscopy

The EIS was used to find the thickness of the film by the following equation

$$\boldsymbol{L_{ss} = \frac{\varepsilon\, \varepsilon_0}{C}}, \qquad (\mathbf{11})$$

where $1/C = -\omega Z''$, w is the angular frequency, Z" is the imaginary part of the impedance.

The Nyquist plots for the various passivation potential is shown in figure 4.5. From all this plot, the value of Z" at the highest frequency i.e. 5 KHz was found and substituted in the above equation to give the value of the reciprocal of the capacitance which was then substituted again in the above equation to give the value of Lss at different passivation potential. The same has been shown in Fig 4.6. Chrono-amperometry was also done at all the above applied passivation potential to study the behaviour of Iss as shown in Fig 4.7. It can be seen that while the value of Lss increases with the increase in the applied potential the value of Iss is predominately constant. This clearly accounts for the validity of the point defect model in accounting the formation and stability of the passive layer.

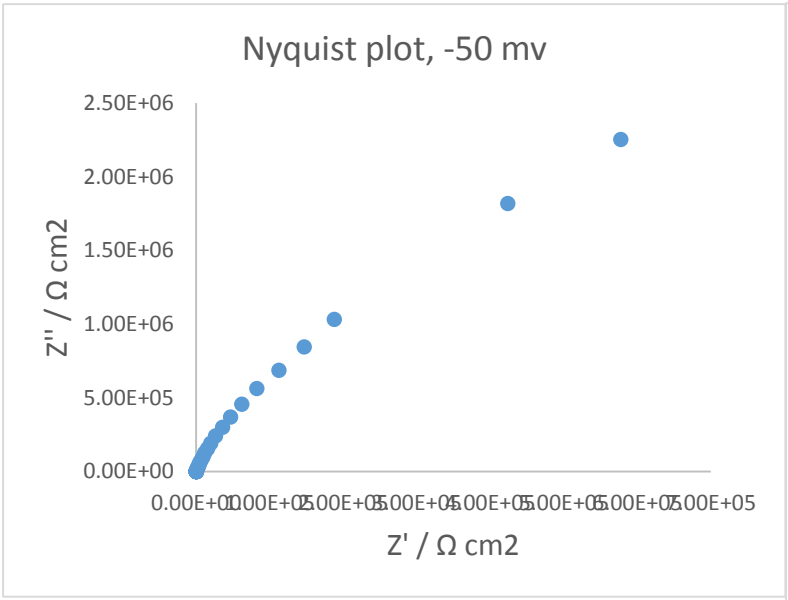

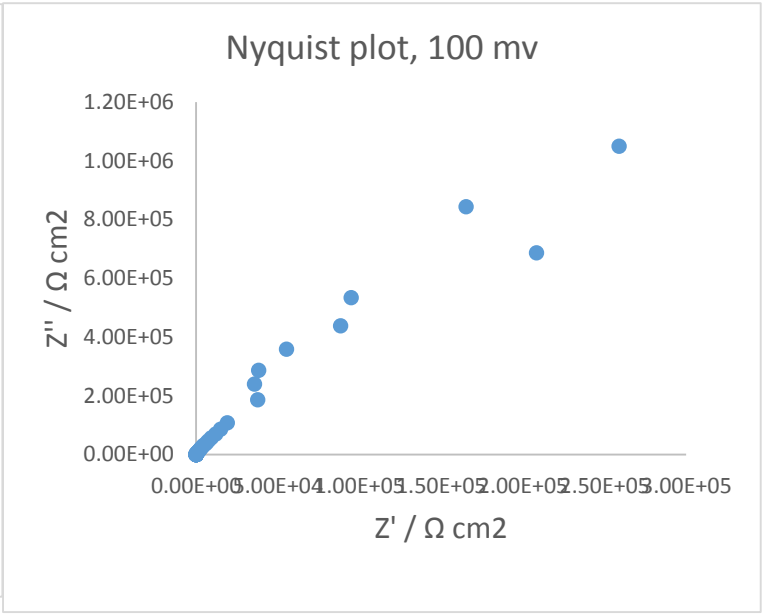

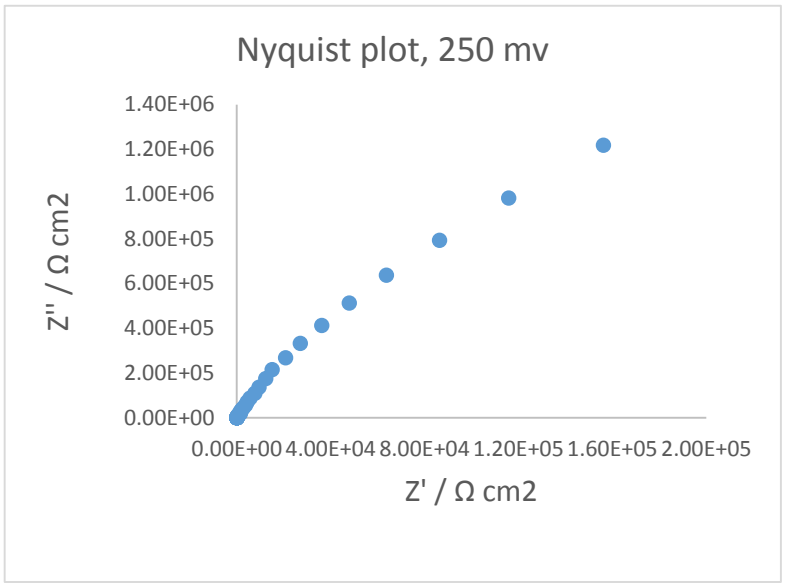

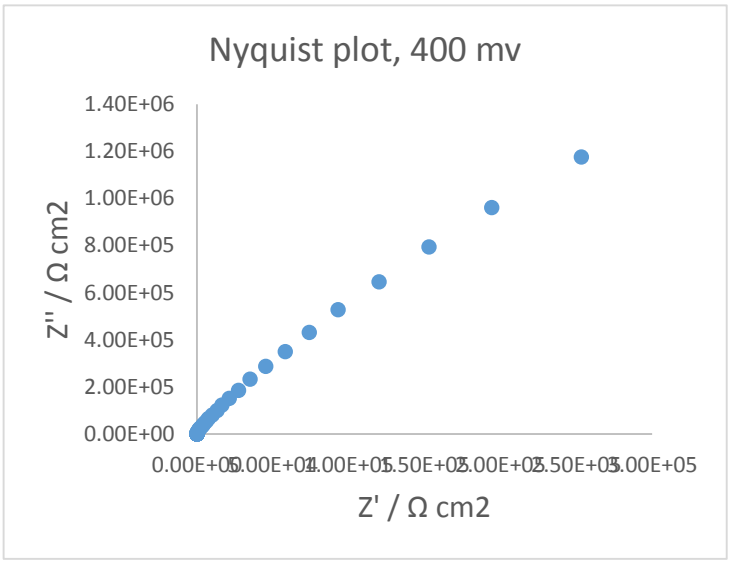

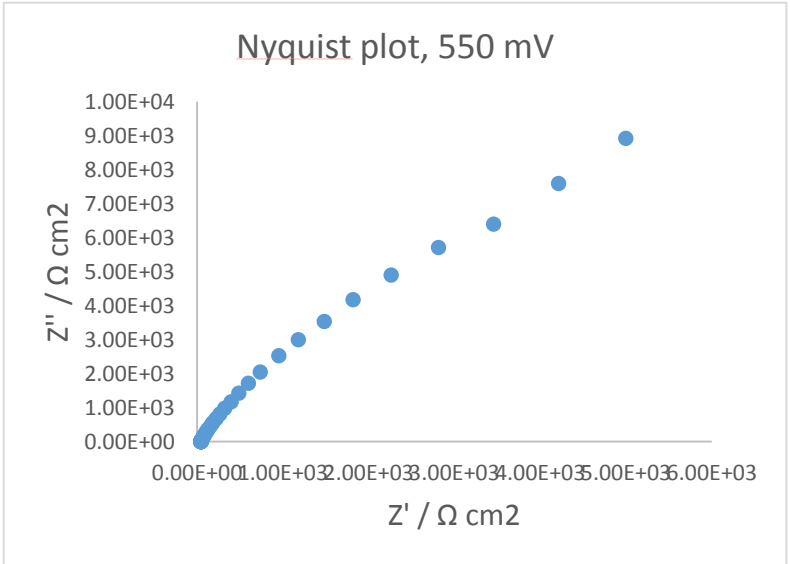

Fig 4.5 Nyquist plots

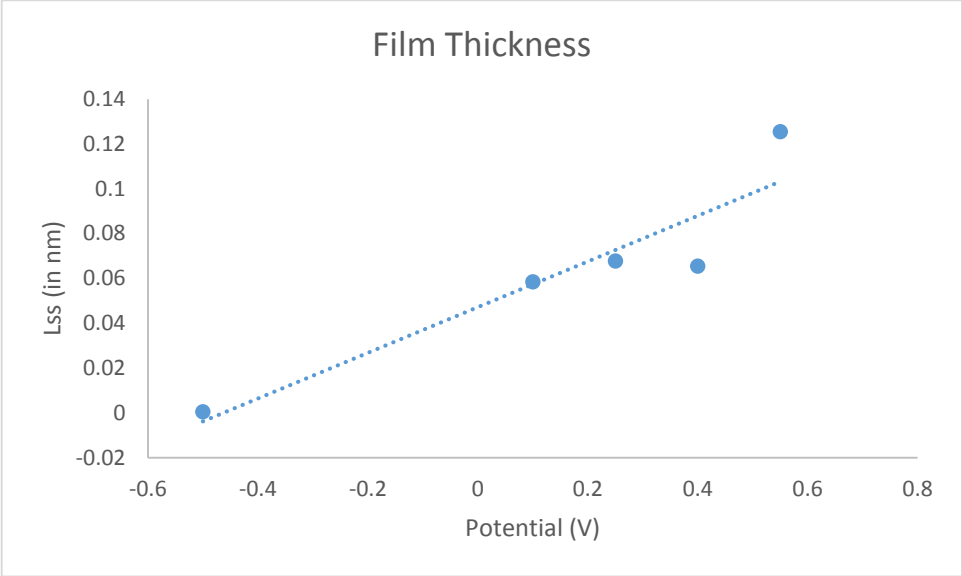

Fig 4.6 Film thickness (in nm) vs. potential V

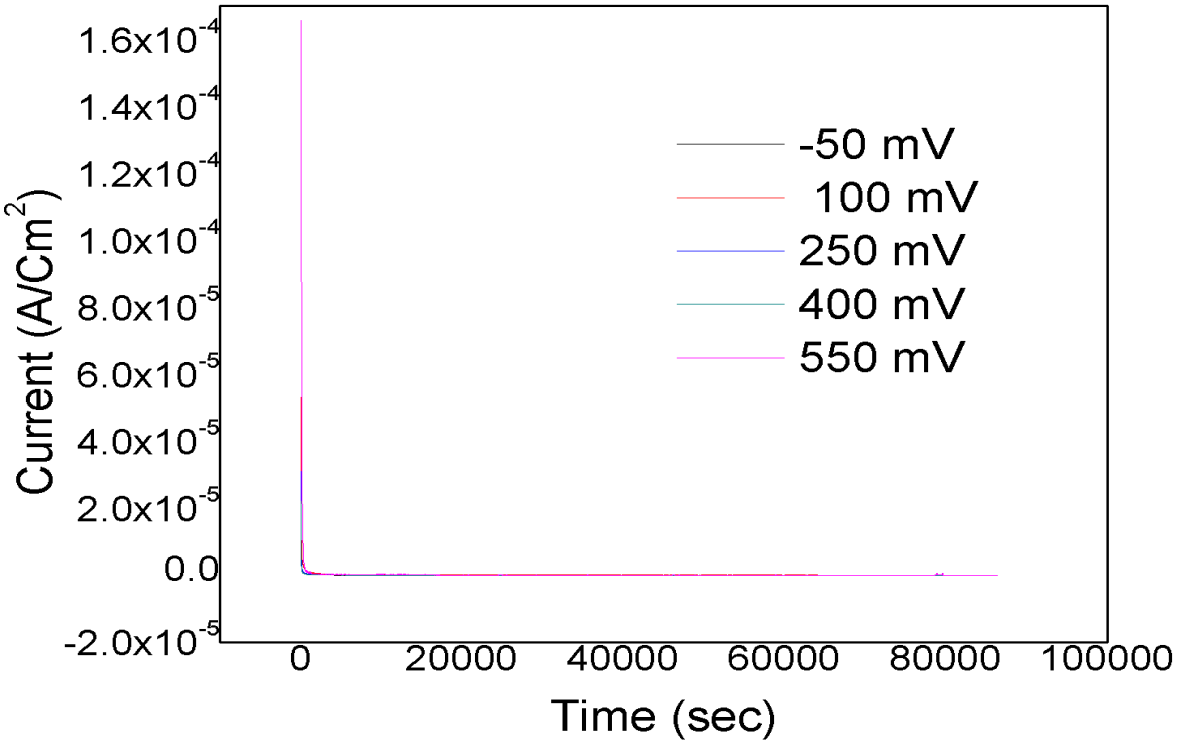

Fig 4.7 Passive Current density vs Time

4.2 Breakdown potential for high manganese carbon steel at ambient temperature

The apparent breakdown potential for the above graded steel is dependent on the chloride concentration which is evident from Eq. 5 above, and decreases with increasing chloride concentration. Fig. 4.8 shows typical potentiodynamic plots in chloride containing borate buffer solution at a potential scan rate of 0.1667mV/s as a function of the chloride concentration. As the potential sweeps in the positive direction, there is a gradual increases in the current density until a region of passivation appears where the current density is almost constant, more positive potential leads to sudden increases in the current density which is a characteristic of passivity breakdown and the potential is known as the breakdown potential [25-29]. The breakdown potential decreases with the increase in the chloride concentration and decreases linearly with the logarithmic of chloride activity as shown in Fig. 4.9.

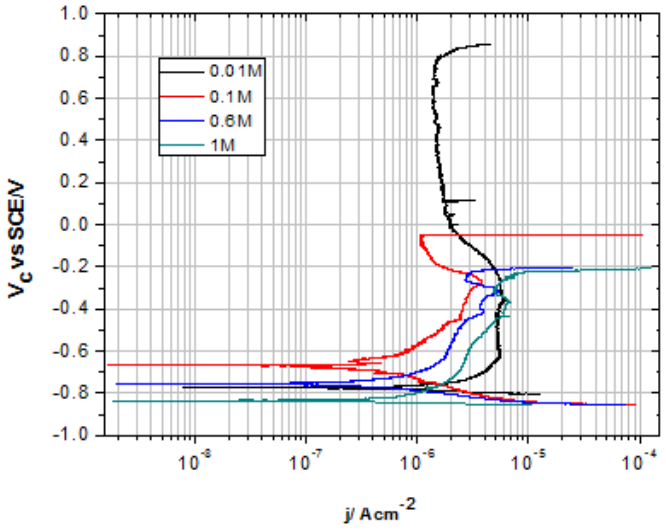

Fig.4.8 Typical potentiodynamic polarization curves (v=0.1mV/s) for high manganese carbon steel in chloride containing borate buffer solution (pH= 10.4 ± 0.1) as a function of chloride concentration at room temperature

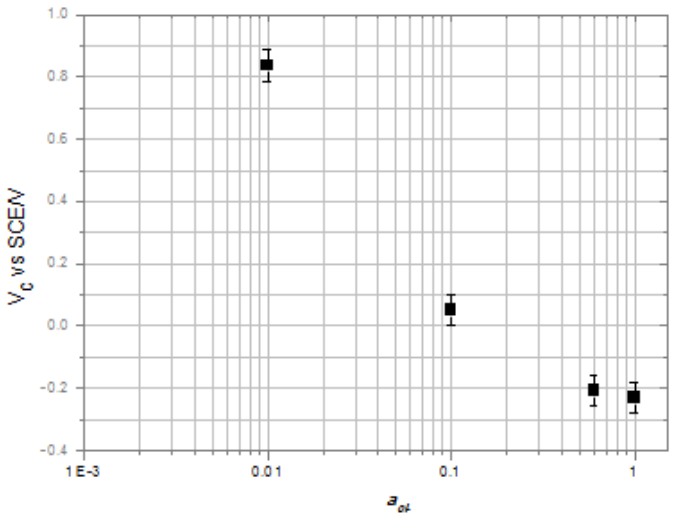

Fig. 4.9 Apparent mean breakdown potentials (υ = 0.1667 mV/s) for type CarElso high manganese carbon steel in deaerated borate buffer solutions (pH = 10.04 ± 0.1) as a function of the logarithm chloride ion activity

Using Eq.53 and the slope obtained from the curve of Fig 4.9, we can determine the value of α, the polarizability of the barrier layer/solution. Slope of the curve = $-\frac{2.303\ RT}{\alpha F}$, substituting the value of R, universal gas constant, T, temperature and F, Faraday constant, gives α = 0.83.

In accordance to the Point Defect Model the breakdown potential (Vc) is dependent on the potential scan rate (v) by the following relation [32]:

$$V_c(v) = (\frac{2\xi RT}{J_m x \alpha F})^{\frac{1}{2}} v^{\frac{1}{2}} + V_C(v = 0) \qquad (12)$$

where ξ is the areal concentration (cm^{-2}) of condensed cation vacancies at the metal/barrier interface that causes the separation of the barrier layer from the substrate metal, leading to passivity breakdown, and J_m is the rate of annihilation of cation vacancies submerging into the metal phase at the periphery of the cation vacancy condensate, V_c (v=0) is defined as the breakdown potential at zero potential scan rate, α is the polarizabilty of the barrier layer/ solution which is determined above by the relationship between V_c and log(a_{cl^-}) as evident from Eq. 5. Fig. 4.10 shows the typical polarization curve at varying potential scan rate. The potential breakdown increases with the increases in the potential scan rate and the current at breakdown

potential also increases with the increase in potential scan rate.

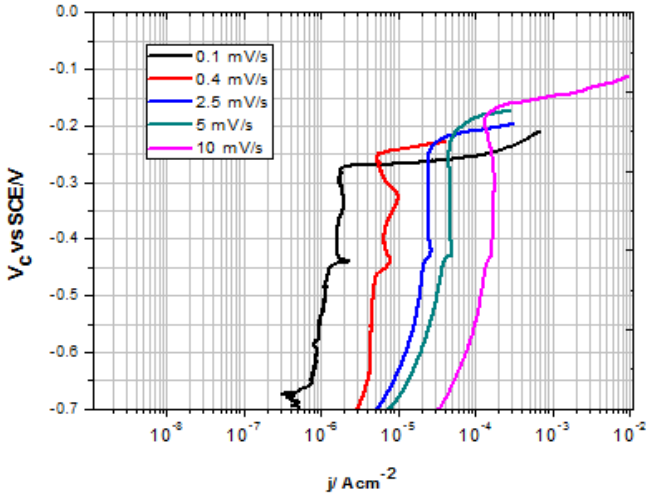

Fig. 4.10 Polarization curves showing dependence of breakdown potential on scan rate

As shown in Fig. 4.11, the measured breakdown potential vs. square root of potential scan rate follows a linear relationship and the slope of this curve is found to be 1.21(V/s)$^{1/2}$, and the value of ξ/J_m = 19.87 seconds. Vc (v=0) = 282 mV. The value of $J_{ca} \leq 2.7 \times 10^{13}$, the critical cation vacancy concentration was found from the following equation

$$J_{ca} \leq \frac{I_{ss} N_v}{xF} \qquad (9)$$

N_v is Avagadro constant, *x* is the valence state of the cation vacancy, I_{ss} the passive current density which is a measure of the annihilation rate J_m and F is the Faraday constant. Thus, Jm= 2.7 x 10^{13} and ξ= 4.9 x 10^{14}. The value of ξ obtained from the structural arguments lies in the range of ~10^{14} which falls well in agreement with the value estimated from the relationship between Vc(v) and $v^{1/2}$. This gives sufficient proof for the validity of point defect model in addressing the passivity breakdown of the passivated layer on high manganese carbon steel.

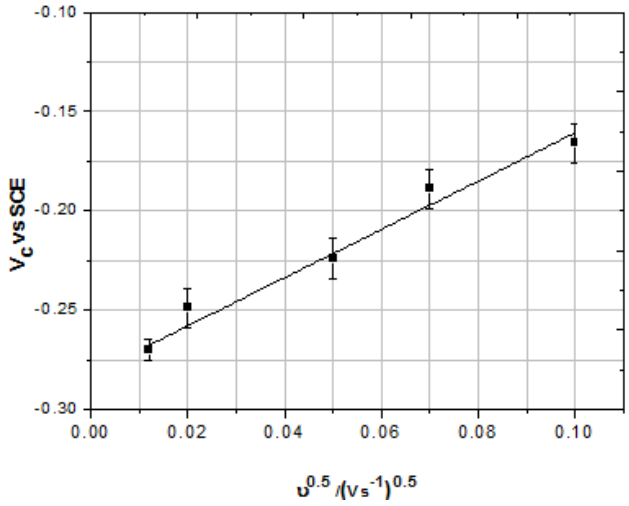

Fig. 4.11 Apparent breakdown potential(v= 0.1667 mV/s) for type high manganese carbon steel in deaerated borate buffer solutions with 1M Nacl as a function of potential scan rate

4.3 Calculation of breakdown potential and its distribution

The Point defect model predicts the formulation for finding the distribution of breakdown potential which follows a normal distribution of potential breakdown sites with respect to cation vacancy diffusivity D characterised by a mean value $\overline{D}$(the mean cation vacancy diffusivity) and a standard deviation σ_D (width of the distribution), as large number of breakdown sites exist in the barrier layer per unit area. There exist a certain critical cation vacancy concentration that leads to the disruption of the passivated layer, which comprises of large number of structural defects. The PDM follows an analytical distribution function for V_c as given in Eq. (8). The cumulative frequency distribution of the breakdown potential, P (V_c), is expressed as Eq. (9) representing the percentage of all breakdown potential that are less than V_c [31].

The potentiodynamic plots at different pH [5.9, 8.2, 9.04, and 10.02] each were carried out for 20 times to plot the cumulative probability distribution of breakdown potential as shown in Fig 4.12. The breakdown potential obtained in each plot was noted and copied to excel document. The same was done for all the above mentioned pH. Then the cumulative probability distribution was plotted as shown in figure 4.13

Using the parameters α, β, ξ, σ_D from Table 1 and substituting them in Eq.8 and Eq. 9, the modelled cumulative frequency distribution of the breakdown potential were designed and compared with the analytically observed data at different pH as shown in Fig. 4.14

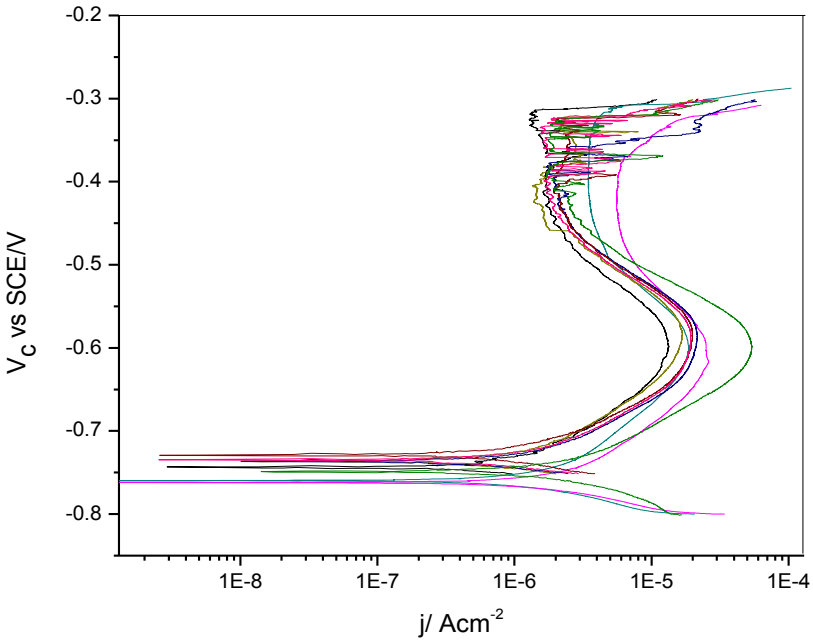

Fig 4.12 Potentiodynamic plots at pH=8.2 for 20 times to plot cumulative probability distribution

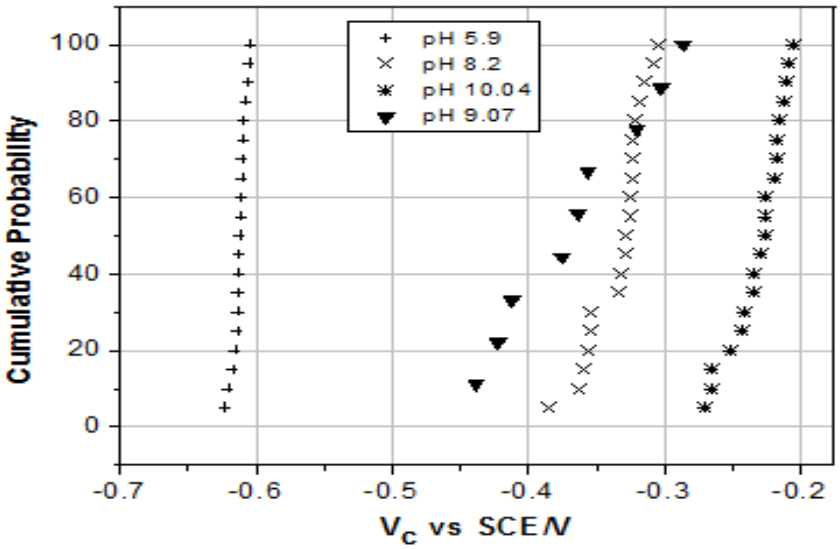

Fig 4.13 Cumulative probabilities in the breakdown potential for Type high manganese carbon steel in deaerated borate buffer solutions containing 1M NaCl with different pH

Table 4.3. Parameter values used in calculating cumulative probabilities in the breakdown potential for carbon steel in deaerated borate buffer solutions containing 1M NaCl at room temperature

Parameters	Value	Unit
F, Faraday constant	96487	C mol^{-1}
R, the gas constant	8.314	J $(mol\ K)^{-1}$
T, the absolute temperature	295	K
N_v, Avogadro's number	6.023×10^{23}	mol^{-1}
χ, the barrier layer stoichiometry (Fe_2O_3)	3	
Ω, molar volume of Fe_2O_3 per cation	15.23	$cm^3\ mol^{-1}$
$\overline{D}$, the mean cation vacancy diffusivity	2×10^{-17}	$cm^2\ s^{-1}$
σ_D, the standard deviation for D	1×10^{-17}	$cm^2\ s^{-1}$
α, potential dependence of $\varphi_{f/s}$	0.83	
ε, the electric field strength	3×10^{6}	V cm^{-1}
ξ, the critical vacancy concentration	4.9×10^{14}	cm^{-2}
J_m, the critical vacancy flux	2.7×10^{13}	$cm^{-2}s^{-1}$
β, pH dependence of $\varphi_{f/s}$	-0.01	V
$w = \frac{\chi}{2}\Delta G_A^0 + \Delta G_S^0 - \frac{\chi}{2}F\varphi_{f/s}^0$	-35.148	kJ mol^{-1}

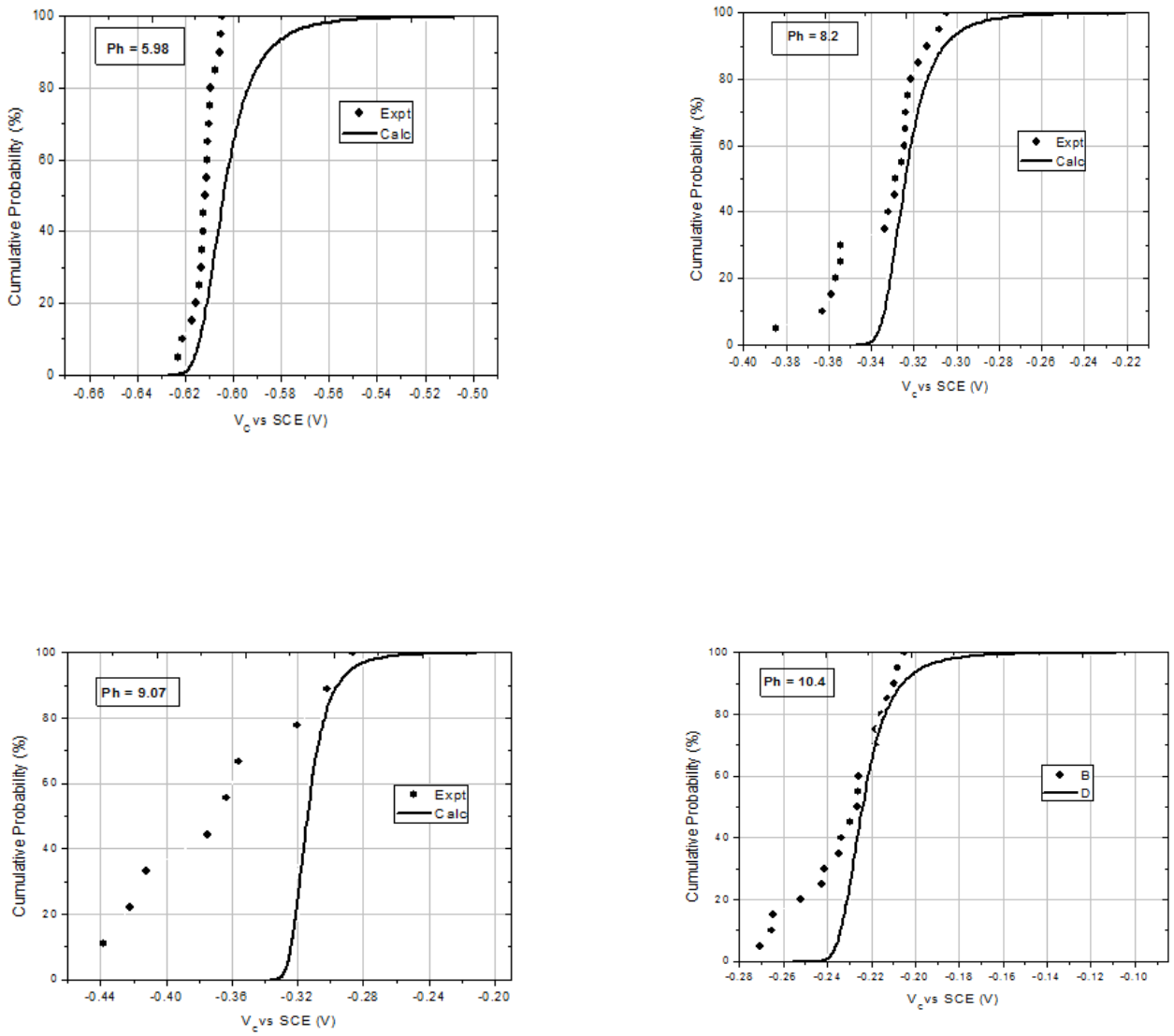

Figure 4.14. Calculated cumulative probabilities in apparent breakdown potential, (0.1667 mV s^{-1}), for Carbon steel in deaerated borate buffer solutions containing 1M NaCl with different pH, compared with the relevant experimental ones at RT. The solid lines are calculated results, and the marker points are experimental data. σ_D= 0.5

4.4 Dependence of breakdown potential of high manganese steel on pH

Fig. 4.15 shows the dependence of breakdown potential on pH. At pH = 5.98, the current increases with the increase in the potential without showing any prominent passivation region as compared to higher pH which shows evident passivation and breakdown potential. The breakdown potential was highest for pH= 10.04. The following behaviour of breakdown potential with respect to pH can be justified by Eq. 5 and 6 above.

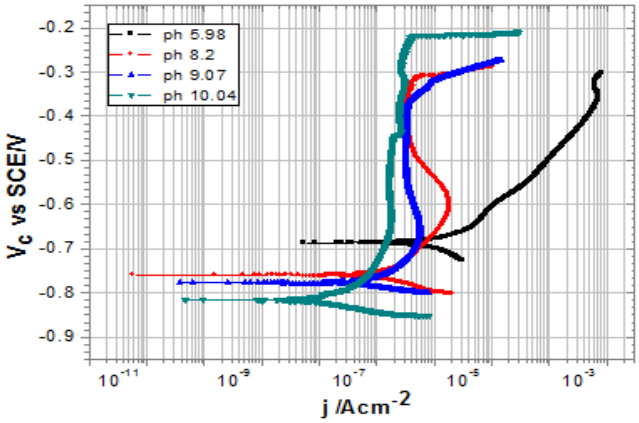

Fig. 4.16 Potentiodynamic polarization curves (v= 0.1667 mV/s) for type high manganese carbon steel in deaerated borate buffer solutions as a function of pH

A plot of breakdown potential with respect to pH gives the value of β, pH dependence on $Ø_{f/s}$. the slope of the plot gives the value of $-\frac{x}{2}\beta F$, where x = 3 and F is the Faraday constant. Fig. 4.16 shows the breakdown potential with respect to pH and the slope calculation gives the value of β~0.01.

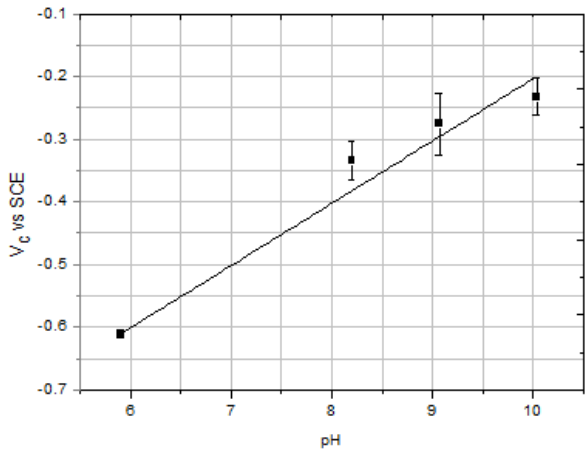

Fig. 4.16 Apparent breakdown potential (v= 0.1667 mV/s) for type high manganese carbon steel in deaerated borate buffer solutions with 1M Nacl as a function of pH.

4.5 Microstructural analysis of pitting corrosion on high manganese carbon steel

The microstructure of high manganese carbon steel in deaerated borate buffer solutions containing 1M NaCl with different pH at a magnification of 10X is shown in Fig. 4 17. The pits formed during the experiment are clearly visible in the optical micrographs. The corrosion products are formed on the silhouette of the pit. The pits can be stable or metastable depending on the environmental conditions.

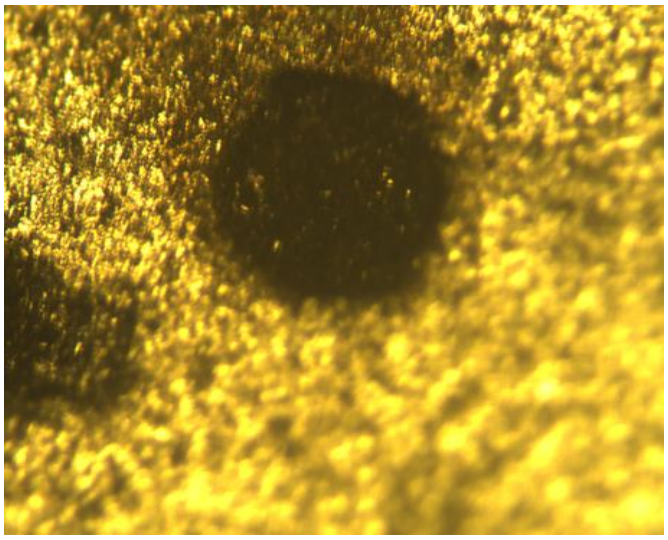

pH= 5.9

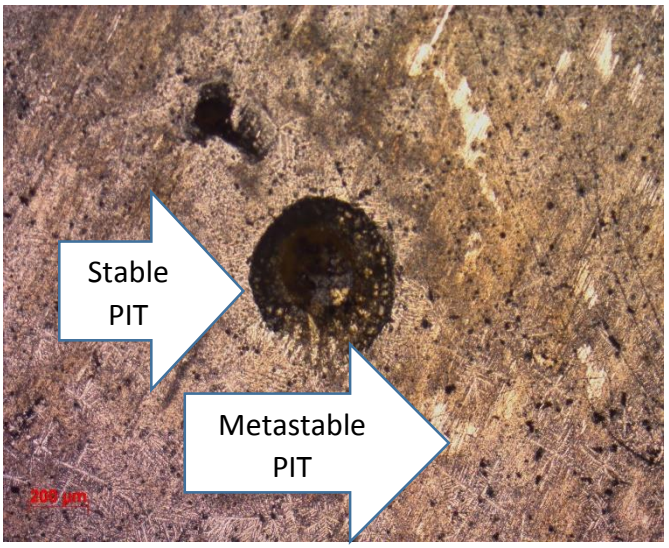

pH = 8.2

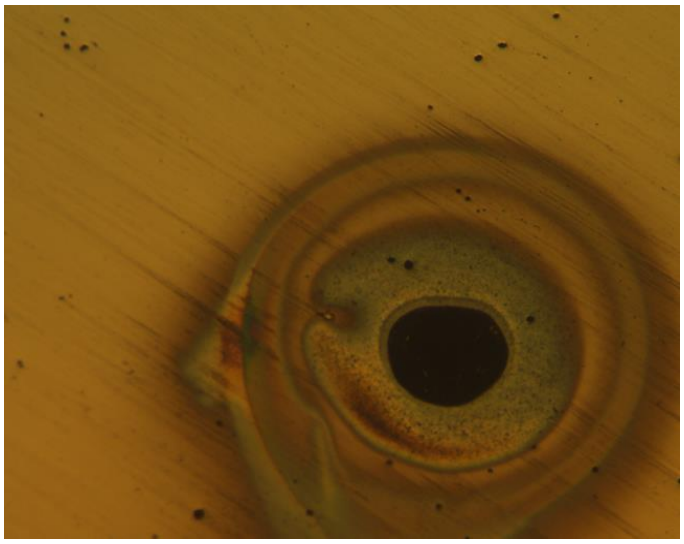

pH = 9.07

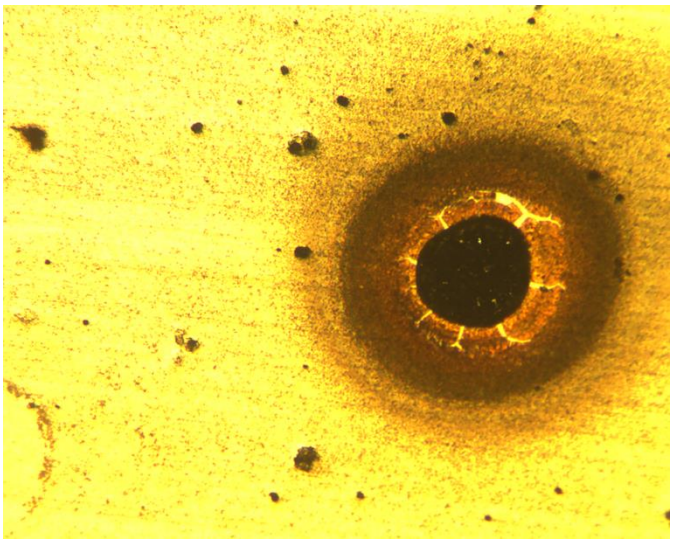

pH = 10.2

Fig 4.17: Micrographs of high manganese carbon steel in deaerated borate buffer solutions containing 1M NaCl with different pH at a magnification of 10X

Chapter 5
Conclusion

5.1 Summary

The present study focuses on the passivity and pitting corrosion of high manganese carbon steel in chloride containing borate buffer solution. Firstly, extensive pitting corrosion is done on the surface of the carbon steel at different pH and chloride concentrations, following which optical micrographs are obtained for the pitting corrosion.

- The passive film was found to have n-type defect structure with thickness of the film less than 1nm. The Iss, passivation current density, was found to be independent with the passivation potential while the Lss, thickness of the film, was less than 1 nm, increases with increases in the passivation potential..
- Carbon steel readily pits in borate buffer. Pitting follows the predictions of the PDM with the critical pitting potential (CPP) being near-normally distributed. The current work is developing a database of values for PDM parameters that will eventually allow us to predict the probability of overpack failure due to pitting at the repository horizon.

- The breakdown potential Vc was found to decrease in value with increasing chloride ion concentration as predicted by the Point defect model. The same behaviour for Vc was also seen with decreasing pH. At higher pH the breakdown potential is higher and decrease with the decreasing pH. The breakdown potential also increased with increasing scan rate.
- Experimental relationships between the breakdown potential (Vc) and the pH, chloride activity, and potential scan rate yield parameters in accordance to the point defect model for modelling the passivity breakdown on high manganese carbon steel. The analysis of the dependence on the breakdown potential on the chloride ion activity yield the value of $\alpha = 0.83$, the polarizabilty of the barrier layer/ solution interface.
- The dependence of Vc on pH yields the value of $\beta = 0.01$, the potential dependence of film/barrier layer on pH.
- The critical vacancy concentration ξ necessary for passivity breakdown was found to be in the range of 4.9×10^{14} for high manganese carbon steel in deaerated borate buffer solution, as determined from the dependence of apparent breakdown potential on the potential sweep rate in reference to PDM. The value of critical vacancy concentration was in good agreement with the value estimated structurally.
- The experimentally determined near normal distribution of the apparent breakdown potential at different pH was found to be following with a little deviation to the curves determined from the theoretical or modelling approach using PDM for high manganese carbon steel. This deviation can be accounted by considering the adsorption of the borate ions present in the solution by the film.
- The optical micrographs shows stable and metastable pits with corrosion products formed on the silhouette of the pit
- Even though the corrosion potential may be significantly lower than the mean CPP, the probability that pits will nucleate is low, but it is not zero. Thus, given the long exposure time (100,000 years), a low probability of pit nucleation can result in significant pitting, but needs an extensive and critical analysis before drawing a definite conclusion.

References

[1] H. H. Uhlig. Passivity of Metals (R. P. Frankenthal, J. Kruger, eds), p. 1. The Electrochemical Soc., Princeton, NJ, 1978.

[2] N. Sato. Passivity of Metals (R. P. Frankenthal, J. Kruger, eds), p. 29. The Electrochemical Soc., Princeton, NJ, 1978.

[3] C. Wagner, pp. 751 to 764, Vol. 5, Corrosion Science, 1965

[4] M. Pourbaix. Atlas of Electrochemical Equlibria. NACE-International, Houston, TX 1973.

[5] G. S. Frankel. J. Electrochem. Soc. 145, 2186, 1998.

[6] J.H. Payer, W.K. Boyd, D. B. Dippold et. al, Mater. Perform., 393, May-Nov 1980.

[7]M.G Fontana, Corrosion Engineering, 3rd ed., McGraw- Hill, New York, p. 1-5, 1986.

[8] H. Kaesche, Metallic Corrosion, R. A. Rapp, transl., NACE, Houston, 1985.

[9] Denny A. Jones, Principles and prevention of corrosion, 2nd ed., Prentice hall, New Jersey, p 220-225, 1992.

[10] D. A Jones, Corrosion processes, R. N. Parkins, ed., Applied Science, Englewood, NJ, p. 180, 1982.

[11] K. E. Heusler and L. Fischer, Werkst. Korros., Vol. 27, pp. 551. 697. 1976

[12] H. Uhlig, Passivity of Metals, The Electrochemical Society, Princeton, p. 68, NJ, 1978.

[13] D.D. Macdonald, Pure Appl. Chem. 71, 951, 1999.

[14] C. Chao and S. Smialowska, Sur]. Sci., 96, 426 1980.

[15] N. F. Mott, Trans. Faraday Soc., 43, 429 (1947); J. Chim. Phys., 44, 172, 1947.

[16] N. Cabrera and N. F. Mott, Rep. Prog. Phys., 12, 163, 1948.

[17] N. Sato and M. Cohen, This Journal, 111, 512, 1964.

[18] D. D. Eley and P. R. Wilkinson, Proc. Roy. Soc. (London) Ser. A, 254, 327, 1960.

[19] D. D. Macdonald and B. Roberts, Electrochim Acta, 23, 557, 1978.

[20] L.-F. Lin, D.D. Macdonald, C.Y Chao, J. Electrochem. Soc. 128, 1187, 1981;
L.-F. Lin, D.D. Macdonald, C.Y Chao, J. Electrochem. Soc. 128, 1194, 1981;
L.-F. Lin, D.D. Macdonald, C.Y Chao, J. Electrochem. Soc. 129, 1184, 1982.

[21] D.D. Macdonald, H.H. Uhlig Award Lecture, The Electrochemical Society Spring Meeting, San Francisco, CA, May, 2001.

[22] D.D. Macdonald, S.R. Biaggio, H. Song., J. Electrochem. Soc. 139 ,170, 1992.

[23] D.D. Macdonald, Proc. Int. Workshop Pred. Long Term Corros. Behav. Nucl. Waste ysts., Cadarache, France, November 26–29, 2001. Euro. Fed. Corros. Publ., in: D. Ferron, D.D. Macdonald (Eds.), no. 36, 2003.

[24] D.D. Macdonald, Pure Appl. Chem. 71, 951, 1999.

[25] D. D. Macdonald, J. Electrochem. Soc. 139, 3434, 1992.

[26] P. Park, M. Urquidi-Macdonald, D.D. Macdonald, ICONE, Hyatt Regency Crystal City, Arlington, VA, USA, April 25–29, 2004, Paper ICONE12-49098, 2004.

[27] H. Tsuchiya, S. Fujimoto, O. Chihara, T. Shibata, Electrochim. Acta 47, 4357, 2002.

[28] D.D. Macdonald, A. Sun, N. Priyantha, P. Jayaweera, J. Electroanal. Chem. 572, 421, 2004.

[29] Digby d. Macdonald, Electrochimica Acta 56, 1761–1772, 2011

[30] J. Liu, B. Marx, D.D. Macdonald, in: P. Wang, T. Zachry (Eds.), Nuclear Waste Management: Accomplishments of the Environmental Management Science Program, ACS Symposium Series 943, American Chemical Society, Washington, DC, 2006.

[31] Yancheng Zhang, George R. Engelhardt et. al., Corrosion Science 48, 3812-3823, 2006

[32] Takumi Haruna, D.D. MacDonald, J. Electrochim. Soc., No. ,1574-1578 May 1997